The sea-level spectrum of cosmic rays at large zenith angles

J.E. Allen

THE SEA-LEVEL SPECTRUM OF COSMIC RAYS AT LARGE ZENITH ANGLES

by

J. E. ALLEN

Presented in candidature for the degree of
Doctor of Philosophy of the University of Durham

Whitsun 1961

PREFACE

The material presented in this thesis concerns measurements made with an emulsion spectrograph of the differential momentum spectrum at sea-level of cosmic rays arriving from large zenith angles in the momentum range 1 - 100 GeV/c. The work has been carried out in collaboration with Dr. A.J.Apostolakis.

Following a short introductory chapter, an outline is given of the basic principles of the technique. This precedes an account of the construction of a spectrograph and of exploratory experiments performed with it. The consequent improvements in design are described and after some theoretical considerations of the origin and propagation of μ-mesons in the atmosphere, the results of experimental measurements obtained with a new spectrograph are presented and compared with the theoretical predictions.

These are the first detailed investigations of cosmic rays, either experimental or theoretical, to be carried out at large zenith angles.

CONTENTS

CHAPTER 1

INTRODUCTION

1.1 The Cosmic Radiation

Since the first discoveries some fifty years ago, there has been a continuing interest in the cosmic radiation and it is now the subject of a very wide field of study. The origins in the universe of this natural phenomenon are as yet in the realms of plausible speculation but much is known of the nature and properties of the primary radiation incident at the top of the earth's atmosphere.

The radiation arrives isotropically and it is composed largely of protons with a considerable fraction of α-particles and a small number of nuclei of heavier elements up to iron and possibly beyond. Their energies range from about 10^8 to 10^{19} eV, the lower limit depending on the latitude, and the number of particles falls off as about the third power of the energy. The primary particles are absorbed rapidly in the upper layers of the atmosphere: the radiation observed at sea-level is almost entirely composed of the secondary and later products of their interactions. In the interactions are produced nucleons, π- and K-mesons and other strange particles with smaller numbers of α-particles and heavier fragments. The more energetic of these make

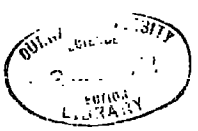

further interactions with similar results, thus the energy of the primary particles is dissipated by being shared out over a much larger number of particles.

A small fraction of protons and neutrons reaches sea-level, contributing to the hard component, but the greater part of this consists of weakly interacting μ-mesons arising from the decay of π- and K-mesons. Photons from the decay of neutral π-mesons give rise to the rapidly multiplying electron cascades of the soft component.

Direct study of the primary radiation is necessarily difficult since it involves the transport of elaborate apparatus to high altitudes of about 100,000 ft (30 km). Nuclear emulsions are fairly easily carried to such heights by balloons in flights of a few hours' duration and it is in this way that the composition of the primary radiation has been determined. Other studies concern the interactions of the very energetic primaries with emulsion nuclei. However, information concerning the energy distribution of the primary radiation comes from a theoretical analysis of measurements of this distribution at sea-level. As will be shown in chapter 5, it is possible to obtain a differential equation relating the intensity of μ-mesons at any point in the atmosphere with the energy spectrum of the parent mesons near the top of the atmosphere. Further assumptions concerning the form of the interactions of the primary particles enable estimates to be made of

the primary spectrum itself.

1.2 μ-meson Momentum Spectra at Sea-level

One particular aspect, then, of the study of cosmic rays at sea-level is the investigation of the momentum spectrum of the μ-meson component. A large amount of experimental work has established this with some certainty for particles arriving from the vertical direction in the range 0.5 to 100 GeV/c and to a lesser degree up to 1000 GeV/c. The investigations have mostly employed a powerful magnetic field in which the particles are deflected, with trays of detectors at different levels to determine the trajectory. Other counter trays in anticoincidence eliminate spurious and undesirable events such as extensive air showers. Often cloud chambers provide increased resolution at the upper end of the energy spectrum. Quite complex electronic circuitry is involved in this type of apparatus although it is a simple matter to observe large numbers of particles with it.

The most recent determination of the differential spectrum has been carried out at Durham by Ashton et al (1960), who made use of close layers of a new type of small counter, the neon flashtube, which permits a more accurate reconstruction of the particle trajectory. They observed some 160,000 particles and their measurements extend from 1 to 2,000 GeV/c. Their results will be referred to later on

in the theoretical calculations.

Less work has been done at directions inclined to the vertical. Interest in measurements of spectra at these angles arises since it is predicted that there should be significant differences between them and the vertical spectrum. It has been shown by Jakeman (1956), Smith and Duller (1959) and others, that an increase is expected in the flux of high energy particles (above about 100 GeV), although the total intensity is very much reduced by the increased depth of the earth's atmosphere. Thus the median energy of μ-mesons at sea-level increases with zenith angle and a study of high energy particles is more profitably carried out at large zenith angles. It has also been suggested that calculations on the sea-level spectra would enable an estimate to be made of the relative proportions of π- and K-mesons giving rise to the μ-meson component. A further important application of the observation of cosmic ray spectra at several zenith angles is that they provide a means of testing models of propagation in the atmosphere of the meson component. Thus having obtained an estimate of the π-meson production spectrum from measurements of the sea-level spectrum in the vertical direction, it is possible to predict the sea-level spectra at other zenith angles using the same theoretical model and to check these against experimental observation.

The first investigations were those of Moroney and Parry (1954) who, with a magnetic spectrograph, carried out measurements of the

differential spectrum at 30° and 60° to the zenith in easterly and westerly directions over an energy range of 0.24 to 70 GeV/c. They compared their results with theoretical predictions based on the vertical spectrum of Caro et al (1951) obtained with the same experimental arrangement. They used a model of extended production in the atmosphere but found poor agreement with the experimental results at 60° which they ascribed to the effects of scattering of μ-mesons in the atmosphere. Their measurements of the positive to negative ratio agreed with theoretical predictions and with the results of Owen and Wilson (1951).

Pak et al (1961) have recently published work carried out at 68° zenith angle in the momentum range 2 to 70 GeV/c. A single π-meson production spectrum accounts both for their differential spectrum and that measured by Pine et al (1959) with an earlier version of the same magnet spectrometer at 0°. It was estimated that most of the μ-mesons observed at sea-level originated from the decay of π-mesons rather than K-mesons. Their values of the positive to negative ratio were in agreement with all previous measurements.

At greater zenith angles the only measurements have been made by Jakeman (1956) and extended by Wilson (1959). Both authors employed trays of shielded Geiger counters to detect particles travelling close to the horizontal direction and to discriminate against extensive air showers and casual coincidences. No estimation of momentum was possible

but the integral rates agreed quite well with theoretical predictions. It was concluded that K-mesons were not an important source of μ-mesons at sea-level.

Thus little is known of the μ-meson momentum spectrum at zenith angles greater than 60° and no measurements have been made over a continuous range of angles with a single technique.

1.3 The Present Experiment

It is seen from the above discussion that a considerable amount of useful information may be expected to be gained from a study of the sea-level momentum spectrum of μ-mesons at large zenith angles. The investigations to be described were carried out with an emulsion spectrograph. This device, for determining the signs and momenta of fast charged particles, was first used by Apostolakis and Macpherson (1957 a,b), hereinafter referred to as I and II. The spectrograph as developed by them had a geometry very suited to the determination of cosmic ray spectra provided that appropriate modifications were made to the design.

Standard methods of momentum measurement by means of the multiple scattering of tracks in nuclear emulsion are in general limited by spurious scattering to momenta below about 10 GeV/c. Attempts have been made to employ magnetic fields in conjunction with emulsions,

but measurement of the deflection of tracks is hampered by scattering and distortion and an upper limit is set of a few GeV/c. With the present technique, the effects of distortion have been eliminated and scattering is very much reduced: momenta as high as several hundreds of GeV/c have been determined.

The momentum is determined from measurements on the curvature of a particle trajectory in a magnetic field. Thin glass plates coated on both faces with nuclear emulsion and separated by large air gaps are supported parallel to each other at equi-spaced intervals in a magnetic field which is directed in the plane of the plates. The tracks of particles passing through the stack close to the normal direction are located in each emulsion and their trajectories reconstructed. This arrangement is termed a normal incidence stack.

There are advantages in employing an emulsion technique as opposed to the more usual counter or cloud chamber methods. Where these methods must contend with spurious triggering of counters or chance coincidences of two or more particles passing through the array, an emulsion technique contains no bias in the selection of the particles observed because of the continuous recording properties of the emulsion. This also means that the experimental measurements are of absolute intensities and normalization of the results is rendered superfluous. Thus an additional check is possible between results obtained by two quite different types of technique.

CHAPTER 2

PRINCIPLES OF THE EXPERIMENTAL TECHNIQUE

2.1 The Normal Incidence Stack

An outline of the theory of the technique can best be given by considering a typical stack consisting of 2m cells, each of length t, formed by 2m + 1 plates (figure 1). The field H, directed along the y-axis, produces a curvature in the x-z plane of the trajectories of charged particles penetrating the stack. A particle of momentum p and incident near to the normal, located in the 1st, (m + 1)th, (2m + 1)th plates, will have a projected magnetic sagitta U_H (assumed small) given by

$$U_H = 1.5\ (mt)^2\ H/p \qquad (1)$$

where U_H is in microns when t is in cm., H in units of 1,000 gauss and p in GeV/c.

Two sources of error determine the accuracy of momenta measured by this method: multiple scattering of particles in the material of the plates and errors of measurement including those in the system of reference. The magnetic sagitta U_H may therefore be regarded as a signal to be measured in the presence of noise.

It is shown in I that the mean square sagitta $\overline{U_s^2}$ due to multiple

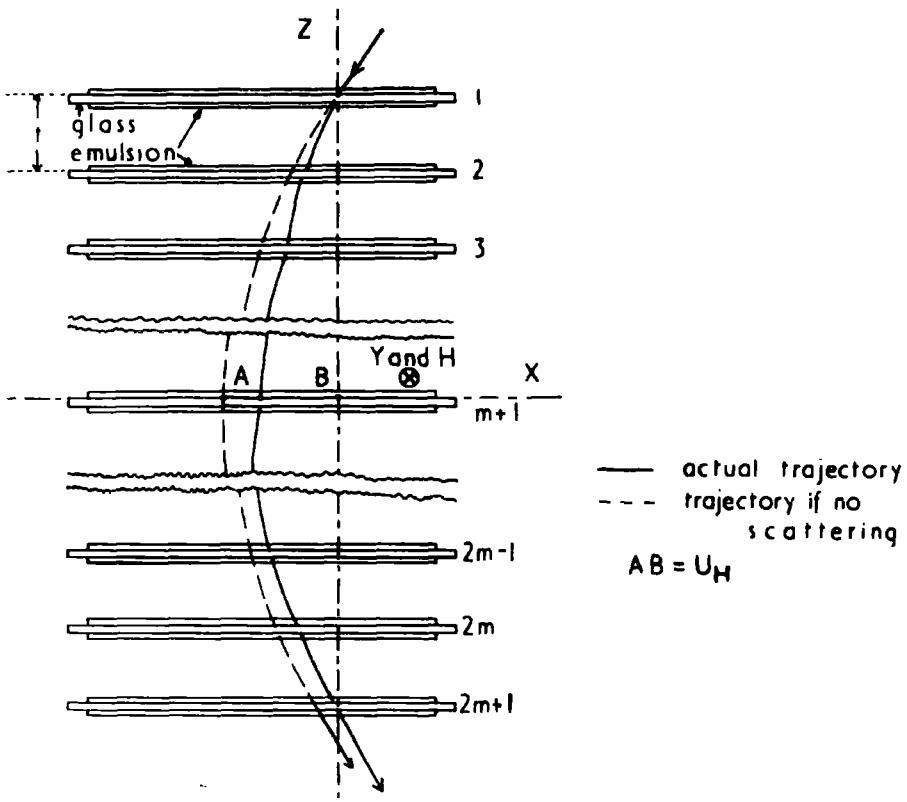

Fig.1. A diagrammatic representation of part of a Normal Incidence Stack to illustrate the basic principles

scattering of a particle located in the 1st, (m + 1)th, (2m + 1)th plates is given by

$$4\,\bar{\bar{U}}_s^2 = t^2\,\bar{\bar{\theta}}^2\left(\frac{2}{3}m^3 + \frac{1}{3}m\right) - \left(t\,\bar{\bar{\theta x}} + \bar{\bar{x}}^2\right)2m \qquad (2)$$

where $\bar{\bar{\theta}}^2$ is the mean square of the projected deflections per cell; $\bar{\bar{\theta x}}$ is the mean value of the product (deflection times lateral displacement) per cell; $\bar{\bar{x}}^2$ is the mean square lateral displacement per cell. The second term is generally small compared with the first. If the root mean square value of the combined errors of measurement is α, then the total root mean square noise is given by $(\bar{\bar{U}}_s^2 + \alpha^2)^{\frac{1}{2}}$. Putting $\bar{\bar{U}}_s^2 = \bar{\bar{U}}_o^2/\beta^2$, the signal to noise ratio is

$$R = U_H\beta\,(\bar{\bar{U}}_o^2 + \alpha^2\beta^2)^{-\frac{1}{2}} \qquad (3)$$

For those particles for which $\beta \doteq 1$ and for $\bar{\bar{U}}_o^2$ large compared with α^2, equation 3 becomes

$$R_o = U_H \,/\, (\bar{\bar{U}}_o^2)^{\frac{1}{2}} \qquad (4)$$

where R_o is a constant independent of momentum.

It may be seen from equations 1, 2 and 4 that, for a given momentum, R_o varies as $m^{\frac{1}{2}}\,t\,H$. Hence for the greatest value of R_o, the magnetic field should be as large as possible, and, for a given length of stack,

a few large cells are better than many smaller cells.

For momenta in the region of 1 - 3 GeV/c the signal to noise ratio R for a typical stack is large. As the momentum increases, both the magnetic deflection and scattering decrease, until errors of measurement predominate, i.e. R becomes less than R_o. A maximum detectable momentum (MDM) is thus defined when R becomes equal to unity; this will occur, for a typical stack, at a few hundred GeV/c. Similarly, for increasingly small momenta, when β becomes $\ll 1$, the signal to noise ratio again approaches unity, at a few tens of MeV/c. In practice, the least detectable momentum (LDM) may be greater than this, owing to difficulty in tracing between plates.

2.2 The Determination of Momentum

A simple method makes use of equation 1, the sagitta U_H being derived from the co-ordinates of the mid-point and ends of the trajectory. The method is suitable for hand computation and is quite accurate for momenta in the region where scattering errors are a small fraction of the signal. Another method affording better precision is that which utilizes the co-ordinates of the trajectory as determined in each plate. The errors on the co-ordinates have a random distribution hence a least squares analysis may be made. This is very laborious in application, but where a digital computer is available there is no advantage in

employing any less accurate method.

For a parabola of the form

$$x = q + rz + sz^2 \tag{5}$$

where the x and z-axes have directions as indicated in figure 1, the curvature in the small angle approximation is

$$\rho \doteq x'' = 2s \tag{6}$$

s is determined from

$$s = \frac{1}{\Delta^2} \begin{vmatrix} \Sigma z_i^0 & \Sigma z_i & \Sigma x_i \\ \Sigma z_i & \Sigma z_i^2 & \Sigma x_i z_i \\ \Sigma z_i^2 & \Sigma z_i^3 & \Sigma x_i z_i^2 \end{vmatrix} \tag{7}$$

where $\Delta^2 = \begin{vmatrix} \Sigma z^0 & \Sigma z_i & \Sigma z_i^2 \\ \Sigma z_i & \Sigma z_i^2 & \Sigma z_i^3 \\ \Sigma z_i^2 & \Sigma z_i^3 & \Sigma z_i^4 \end{vmatrix}$

If the error in each measurement is δ, then the error δs in s is given by

$$\delta s^2 = \delta^2 \Delta_{33}^2 / \Delta^2 \tag{8}$$

where Δ_{33}^2 is the two-rowed principal minor of Δ^2.

The use of a least squares method as compared with the three - point method results in an increase in the signal to noise ratio which depends on the number of plates i.e. points of observation of the trajectory, in the stack. For a typical stack the increase in the MDM is about 1½ times.

2.3 Practical Considerations

Since the basic requirement for momentum determination is the reconstruction of the trajectory of a particle through the stack, it is necessary firstly that the position of any track in each plate be known accurately with respect to a system of reference in that plate, and secondly that the relationship of each plate to a common co-ordinate system be determined. This last requirement implies a calibration of the instrument before exposure, hence accurate reproduction of the position of the plates is of primary importance. Moreover, it is desirable to complete the assembly of the stack very shortly before the commencement of the experiment in order to eliminate as far as possible "no field" tracks; a similar state of affairs applies when the exposure is terminated. Finally, each plate must be prepared and afterwards processed separately.

These considerations have determined the various features of the design of the spectrographs which were constructed.

The first experiment was in the nature of a pilot venture. Use was made of a powerful electromagnet which was available at the time although the configuration of the magnetic field was not particularly suitable. The field was directed so that the deflection of trajectories would be in a vertical plane; thus the acceptance of low energy particles from smaller zenith angles was possible. Later it was found that this defect was very much more serious than had been anticipated. A second series of experiments was carried out with a small permanent magnet and spectrograph designed in the light of the experience gained during the first exposure and with successful results.

Many technical aspects are common to both series of experiments and will be described in detail only once.

CHAPTER 3

EXPERIMENTS WITH THE FIRST SPECTROGRAPH

3.1 The Construction of the Spectrograph

The form of the first spectrograph was determined by the shape of the pole gap into which it was designed to fit. It consisted of seven frames mounted on a supporting structure at intervals of 1.83 cm and an eighth frame at a distance of 1.33 cm from the seventh, the whole construction being of brass. Each frame was 16.7 x 5.0 x 0.6 cm with an upper support 9.0 cm in length and a window 8.0 x 4.0 cm (figure 2). To a shallow step surrounding the window was cemented a thin sheet of glass, 800 μm thick, to both sides of which were attached 100 μm Ilford G5 emulsions.

A kinematic method of locating the frames on the supporting structure was employed (figure 3). The location was provided by a hole, groove and flat arrangement, the complementary members on the frames being steel balls 2 mm in diameter. The holes were cut with a tungsten tipped drill at appropriate intervals into a glass strip of thickness 3/8 in. cemented on one side of the supporting structure and the grooves similarly on the other side. To the underside of the upper supports of each frame were attached the steel balls, one at

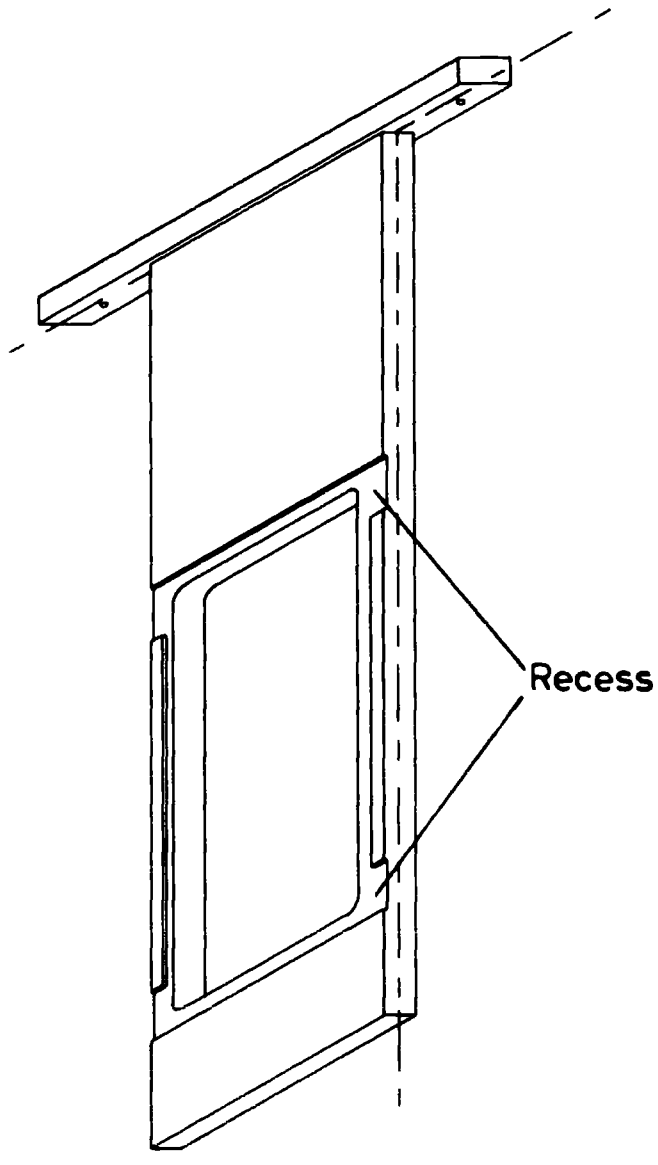

Fig. 2. Isometric drawing of a frame of the first spectrograph.

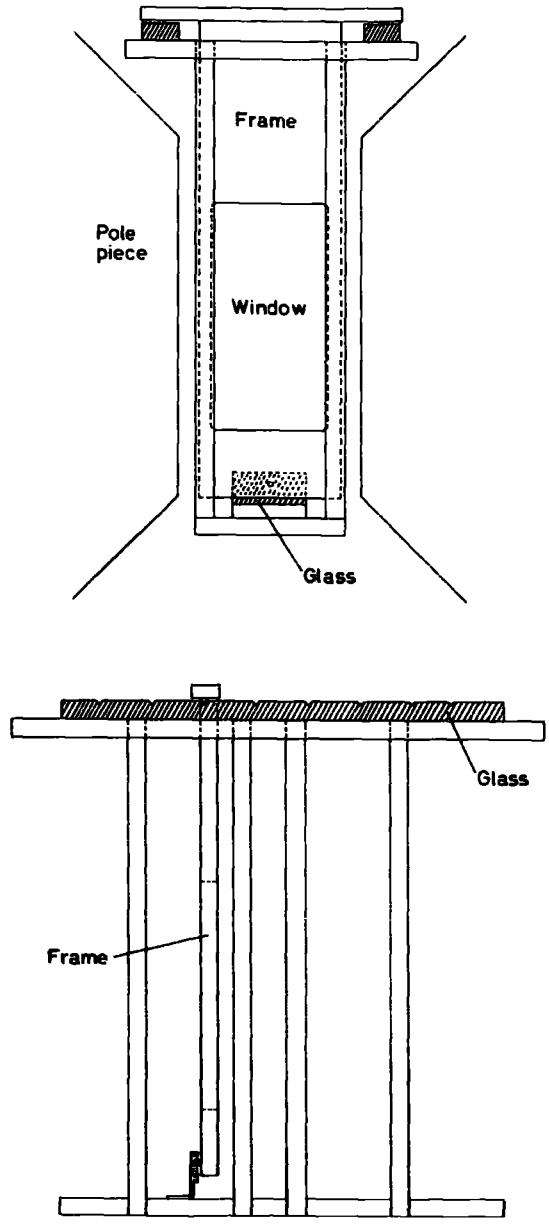

Fig 3. Front and side views of the first spectrograph showing a frame in position on the supporting structure and the arrangement of the magnetic field.

either end, which located into the holes and the grooves. At the lower end of each frame was a third ball which rested against a plane polished piece of glass. The upper support was attached to the frame in a position such that the weight of the frame might cause it to rest against the polished glass flat. The reproduction of the position of the frames on the supporting structure afforded by the kinematic location system was found to be better than $\pm$ 1 μm. Initially both the upper support and lower constraint were moveable so that the frames could be made accurately parallel. Their separations were later measured to within $\pm$ 50 μm with travelling microscopes.

3.2 The Construction and Calibration of the Co-ordinate System

Provision of a common co-ordinate system for the stack was made by engraving with a diamond a rectangular grid on the glass of the plates before the emulsions were attached. The operation was carried out on a milling machine with the diamond in its holder fixed so that it could rotate only in a vertical plane and with the supporting structure placed on end clamped to the carriage. With the last frame in position, a line was drawn by moving the carriage horizontally relative to the diamond. Corresponding lines were then engraved on further frames by building up the stack and lowering the carriage to keep the cutting angle of the diamond constant. In this way a

complete and identical grid of 7 x 3 lines at 1 cm separation was cut on each plate. An elaborate method of construction is required since unless the different lines are accurately parallel to each other with small plate to plate displacements, great difficulty is experienced in the subsequent calibration. The lines were easily visible under a microscope both with a normal dry objective (11x) and under emulsion with an oil-immersion objective (45x). Although some few μm in width, they had a fine structure enabling a setting accuracy of less than 1 μm to be attained.

To complete the co-ordinate system, it is necessary to know the relationship between the lines on individual plates as well as that between corresponding lines on adjacent plates. These mensural operations are defined as calibrations. The former calibration may be performed conveniently on a Cooke M4000 microscope; for the latter, in this particular case, a monocular microscope of highly reproducible translational movement was employed (Apostolakis, 1956). This had been specially designed for the calibration of the vertical stack described in II and the noise level of the instrument was determined as being ± 3.5 μm in 11 cm. Ideally, the translational movement of the microscope should be linear to within 1 - 2 μm, but in practice this is difficult to achieve. However, by rotating either the microscope or the stack through 180° and repeating the calibration process, errors

due to lack of linearity may be eliminated. For a vertical stack, rotation through 180° is simple but with a horizontal stack, it is the microscope that must be rotated. Attempts were made to construct a microscope which could be so rotated but it was found impossible to achieve the necessary precision of movement. The calibration was performed therefore using the vertical microscope already referred to and with the stack placed below having its axis vertical.

The supporting structure was clamped in a rigid outer framework to prevent the creation of any unwanted stresses and was then mounted below the microscope on an optically flat glass plate, the frames being held in position by spring clips. It was ascertained that the clips would not affect the position of the frames. With the microscope focussing on one particular cross in the ruled grid on each plate, the frames were successively removed and co-ordinates from the eyepiece graticule recorded. Because of the accuracy of the engraving, it was possible to use a high power of magnification. The stack was rotated through 180° and the process repeated. The whole operation was carried out for other crosses of the grid and the mean values with their standard deviations computed.

3.3 The Exposure and Development of the Plates

Following calibration, the frames were sent to Messrs. Ilford, Ltd.,

at Ilford where "subbing" was performed, a process which prepares the surface of the glass for the attachment of "stripped" emulsions. Fresh emulsions were employed to reduce unnecessary background.

The length of the exposure of a stack is determined by the available flux of cosmic ray particles. A suitable balance must be struck between a density of tracks so high that confusion arises when tracing trajectories through the stack, and one so low that scanning is made unnecessarily tedious. The first exposure was made with the normal to the plates directed horizontally in the direction of geomagnetic north and it was expected that a one month's duration of exposure would result in a convenient track density.

Because of the long duration of the exposure, however, it was necessary to take precautions against fading of the latent image in the emulsion caused by chemical oxidation and thermal excitation. The stack was therefore sealed in an airtight, light-proof container, with provision made for the circulation of argon of controlled humidity. Throughout the exposure, measurements of the temperature were made by means of thermocouples at four points on the stack in order to detect any existing temperature gradient. Between the container and the pole pieces of the magnet were placed cooling coils for the circulation of refrigerated water which absorbed some of the considerable heat dissipated by the magnet. A temperature inside the container of

between 16 and 17°C and a relative humidity of 60% were maintained throughout the exposure. The stack was shielded from above during the exposure with 10 cm of lead. As short a time as possible was permitted to elapse between the placing in position of the last plate of the stack and the switching on of the magnetic field.

The magnet itself is now incorporated in the Durham Cosmic-Ray Spectrograph (Ashton et al, 1960). Additional pole pieces (see figure 3) were inserted which had been designed to produce as high a field as possible over the volume of the stack (11 x 11 x 6 cm). Each was in the shape of a frustum of a cone, the inner and outer faces of which had diameters 5" and 9" respectively and were separated by a distance of $1\frac{1}{2}$". After the termination of the exposure, the field was measured systematically at numerous points in the volume using a search coil in conjunction with a flux meter and a contour map of the field strength was plotted. The mean value was found to be about 23,000 gauss.

The plates were processed by a temperature cycle method using Amidol developer and they were not detached from the frames until processing was complete. To prevent their being attacked by developer or fixer, the frames were varnished with a solution neutral to the emulsion. At the hot stage, where it was desired to procure a rise in temperature of the plates from 5°C to 22°C within a reasonable

period of time, account was taken of the large thermal capacity of the brass by placing the frames in contact with other similar ones at a higher temperature so that equilibrium would be reached at 22°C.

3.4 The Results of the First Experiment

3.41 Examination Procedure

The tracing of particle trajectories through the stack is begun by searching for suitable pairs of tracks in the two emulsions of the first plate. Since the particles, though of relativistic velocities, are incident close to the normal, they appear in the emulsion as steep black tracks, though these may be curved because of distortion. Tracks are paired from their similar lengths in either emulsion and their same apparent direction at the emulsion-air surface, since this direction is unaffected by distortion.

Prediction of the position of a track in the next plate is possible since there is no slipping between the surfaces of the emulsion and the glass; hence the exact location of a particle is known at two points in each plate and its undeflected direction may be calculated. To facilitate the process further, the first air-gap is made considerably smaller than the cell-length employed in the stack.

Once a particle has been located in two plates a more accurate estimate of its position in the third plate is possible. After this,

tracing through the remainder of the stack presents no difficulty. Confusion between tracks does not arise provided that the particle density is sufficiently low. Moreover, the appearance of any pair of tracks in a plate may be expected to be similar to the corresponding pair of the previous plate, any differences, caused by bending in the magnetic field or by multiple scattering, being proportional to the distance from the predicted position.

3.42 Experimental Results

The examination was carried out on Cooke M4000 microscopes under a magnification of 45 x 1.5 x 15.

It was decided to consider only particles entering the stack at angles of between 80° and 90° to the zenith; thus tracks found in the first plate were accepted or rejected according to their direction as determined there. Also, if the corresponding pair in the second plate showed too great a magnetic deflection, then the particle was not traced further. In practice, tracks were scanned for in both the first and second plates and then traced across the gap.

Of about 100 particles paired in the first and second plates in a total area of 1.8 cm^2 of scanned emulsion only one half had corresponding pairs in the other plate, and of these only a third could be traced through the stack. Concerning the remaining two-thirds, most were deemed as being of such low momentum as to make tracing impracticable, but a number could not be found in any subsequent plate. It may be

noted that no tracks, including those of particles located in all other plates of the stack, could be traced into the third plate. It is, however, an advantage of this technique, that the accidental loss of one of the plates does not vitiate the experimental work and indeed only reduces the accuracy by a very slight amount.

3.43 Analysis of the Results

It had become clear at this stage, with regard to the number of particles found, that the intensity was much smaller than expected. To try to account for this, it was decided to investigate both scanning efficiency and possible movement of some or all of the plates of the stack. The overall scanning efficiency was found to be about 60% and this alone could not account for the reduced intensity. Concerning possible movement during exposure, it had been noticed that all particle tracks traced into the last three plates were systematically displaced from their expected positions. Calculations showed that this could be accounted for by assuming a rotation of the frames in a vertical plane about the upper hole and groove supports. Measurements on the stack confirmed this possibility: supposing that the force exerted by the magnetic field gradient on the lower steel ball had caused these plates to rest against the vertical members of the supporting framework, then the observed angles with the vertical agreed well with those calculated. A rough experiment showed that the gradient of the magnetic field was of the required sign and of just sufficient magnitude for this to have

occurred.

Nevertheless, to account for the apparent low intensity it was necessary to consider a lateral shift of one or all of plates 1, 2 and 4. To test this hypothesis, particles were scanned for in plate 4 and traced into plates 5 and 6. Those appearing in all three plates were then followed back into the first two. Of 18 tracks attempted in this way, all appeared in the second plate, but in the first, 2 did not; thus the possibility of a lateral shift having occurred could not be ruled out. As a result, although the selection of particles would not have been biassed in any way, an estimation of the absolute intensity of particles travelling horizontally became almost valueless. Since the movement of some of the plates would have led to inaccuracies in the determination of momentum, discrimination against particles of low momentum scattered in from smaller zenith angles would not have been possible. Because of the large fringing fields this was thought likely to be a source of considerable error.

In view of the doubt attaching to any results that might have been obtained from this stack, further examination of it was abandoned and instead a second exposure was planned after suitable modifications to the spectrograph had been made.

These modifications included the replacement of the lower steel ball by a brass screw and the introduction of a clamping device to hold the frames in position. In all other respects the details of the

second exposure were similar to the first. Whilst the second exposure was being carried out, however, trial developments showed that the emulsions which had been used exhibited an apparent decrease in sensitivity compared with those of the first exposure. A satisfactory image was obtained only by increasing the duration and temperature of the hot stage. Unfortunately, during the final processing of the exposed emulsions, oxidation of the developer at the hot stage resulted in the almost total loss of the latent image. Examination of this stack was therefore not possible.

Despite the disappointing lack of success, confidence in the technique was felt and it was decided to begin a fresh series of experiments on the basis of the experience gained up to this point.

3.5 Conclusions

The inconvenience of using a large electromagnet for experiments with the spectrograph had become apparent despite the advantage of the high field strengths which could be obtained from it. Any momentary failure of the power supply brought into operation an automatic cut-off switch; thus constant supervision was required in order that, in the event of such a contingency, the current might be restored or one plate of the stack removed so that "no field" tracks could later be distinguished. In practice supervision was maintained for about 18 hours out of each

24, and the three failures which occurred all fell during one of these periods of supervision. In each case it proved possible to restore the power supply within a few minutes.

The large quantity of heat dissipated by the magnet necessitated the carrying out of the exposures at a relatively high temperature with a consequent increased risk of the fading of the latent image. Because of the large volume of space taken up by the winding of the magnet, access to the gap between the poles was very restricted and many delicate operations, such as the placing of the frames on the supporting structure, could be carried out only with extreme difficulty. Had the gap been more accessible, it is probable that the effect of the magnetic field in causing movement of the plates would have been noticed. It is clearly preferable to construct as far as possible an ideal spectrograph and then to design a magnet with which it may be operated, rather than design a spectrograph to fit a pole gap of prescribed and not particularly suitable limits.

A further disadvantage concerned the direction of the magnetic field which was such as to cause deflection of trajectories in a vertical plane. Thus the zenithal angle of arrival of a particle was affected and it was possible for particles to be deflected into the spectrograph from lower zenith angles. This is an important consideration since, as will be shown in chapter 5, at angles near to the horizontal

the cosmic ray intensity falls off very rapidly with increasing zenith angle.

On account of the variable nature of the emulsions, it was thought that a series of exposures of shorter durations would have a greater chance of producing some successful results. With this in mind, the investigations were extended to include smaller zenith angles where the cosmic ray intensity is higher and greater statistics are more readily built up. After much deliberation, it was concluded that a small permanent magnet producing deflections in a horizontal plane would be better suited to the present study, and a new spectrograph and magnet were accordingly designed.

In conclusion it should be added that at the time that these first exposures were performed, the detailed theoretical calculations described in chapter 5 had not been carried out. Estimates of the expected intensity of particles were based on approximate extensions to the calculations of Jakeman. When the investigations were extended to include lower zenith angles, the need for new calculations from first principles became imperative. Subsequently, a comparison showed that the earlier attempts had resulted in a considerable overestimation of the expected intensity. In fact, the number of particles found in the first exposure was too low by a factor of only about 20%. However, the small total number of particles which could have been

obtained from a four weeks' exposure at such large zenith angles in any case made a detailed examination of the stack not worth while.

CHAPTER 4

THE SECOND SERIES OF EXPERIMENTS

4.1 The Design and Construction of the Spectrograph

For the second emulsion spectrograph, the same principle of design was adhered to but the shape of the frames was changed. To secure as high a field as possible with the permanent magnet they were designed to fit a small gap between the pole pieces. The surface area of emulsion was kept approximately the same by making them correspondingly wider. A slightly larger stack was used to help to compensate for the unavoidable loss in field strength.

Seven frames were again employed but spaced at intervals of 2.54 cm and with the eighth 1.00 cm from the seventh. Each frame was $6\frac{1}{2}$ in. x 1 $\frac{7}{16}$ in. x $\frac{3}{8}$ in. with projections of $\frac{3}{8}$ in. on one of the long sides and a central window 5 $\frac{5}{16}$ in. x 1 $\frac{3}{16}$ in. (figures 4 and 5). The sandwich plates were cemented on to the shallow step surrounding the window and additional security was provided by a thin brass plate at either end screwed down to hold the glass. An identical type of kinematic location was used but each frame was held in place by a clamping device assisting the gravitational constraint (not shown in the figure). It consisted of small brass strips screwed to the supporting

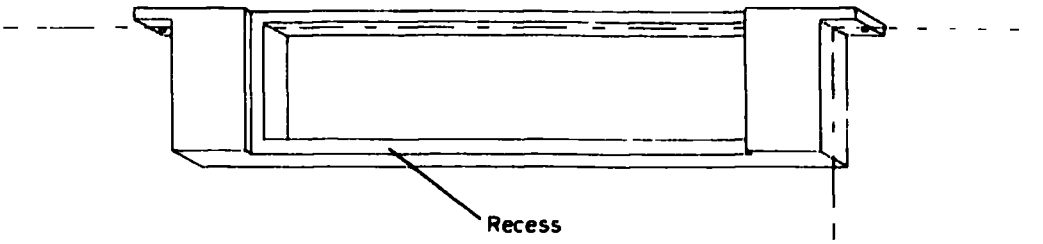

Fig.4 Isometric drawing of a frame of the second spectrograph.

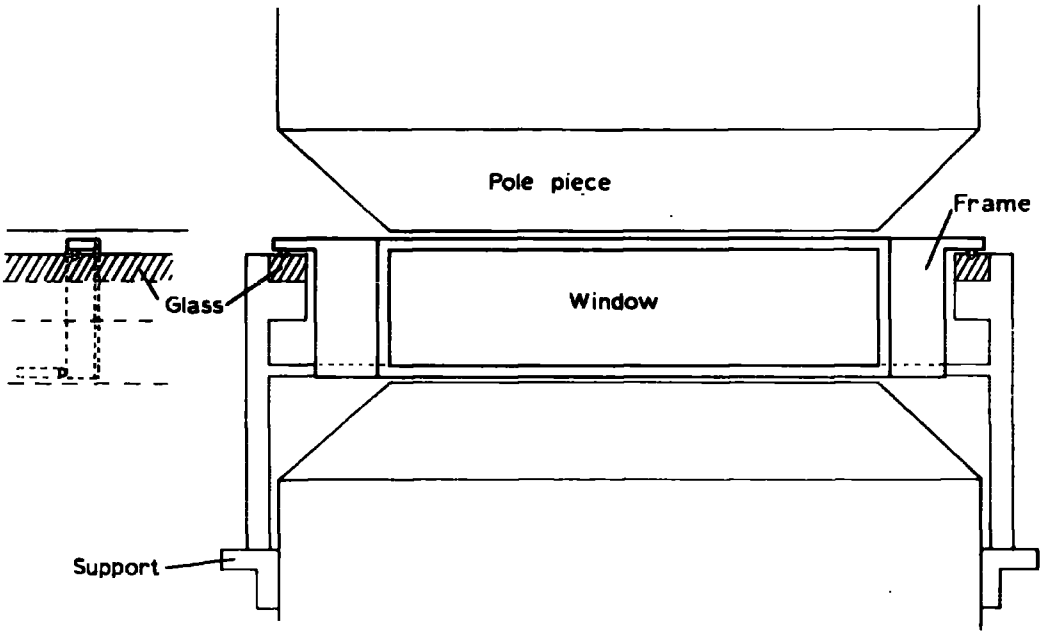

Fig 5 Sectional drawing of the second spectrograph showing a frame on the supporting structure and the position of the pole pieces.

structure one at either side of each frame so that they exerted downward pressure on the upper surface of the frames. A single point of contact was provided by a steel ball 1mm in diameter soldered to the frame. Notwithstanding the additional constraint, the position of each frame was reproducible to better than 1 μm.

By means of an engraving diamond, a reference grid was inscribed on each plate exactly as described in section 3.2. and, using the same vertical microscope, a similar calibration was carried out. The stack had been designed so that no extra support would be required when this was done. The reference grid consisted of a single line down the length of each plate crossed by seven short lines perpendicular to it at intervals of 2 cm. The arrangement of the grid was determined by the area available for examination given by the stage movement of the Cooke M4000 microscopes.

Two complete sets of eight frames were made and the calibration of both was carried out at the same time. This saved time and labour in the setting up of the apparatus necessary for inscribing and calibrating the reference grids and enabled a second exposure in the magnetic field to begin immediately after the termination of the first.

4.2 The Exposure in the Magnetic Field

In all, four exposures in the magnetic field were made; details

are given in table 1.

TABLE 1

No. of exposure	Type of emulsion	Mean inclination	Approximate duration in days
1	G5	75°	14
2	G5	85°	26
3	K5	80°	28
4	G5	85°	49

Column three gives values of the angle between the normal to the plates and the vertical. The durations of the exposures were designed to give a convenient working density of tracks.

The overall dimensions of the magnet were 12" x 18" x 8", each pole face was 6" x 7" and the separation between them was 1½". The design and construction were by Messrs. Swift Levick and Sons Ltd., of Sheffield and the pole pieces were of "Columax" giving a field strength of 6,500 gauss, uniform to within 2% over the volume of the stack. It should be noted that seven plates of the stack cover the whole of the useful volume of the magnetic field; the eighth plate, whose function is to facilitate the tracing of trajectories, is slightly outside this volume. The field was so directed that magnetic deflection took place in the plane containing the long axes of the plates. The normal to the plates was aligned on the geomagnetic meridian such that particles

were accepted from a northerly direction. No contribution was expected at angles near to the horizontal from particles arriving in a southerly direction since a hill, some $\frac{3}{4}$ km in thickness, provided a severe obstruction to such particles having angles of incidence greater than 80° to the zenith. The inclination to the horizontal was achieved by inserting wedges of the required angle underneath the magnet. The angle was measured accurately with a clinometer by extending the plane of the lower pole face with a plane glass sheet.

As in the earlier experiments, the volume containing the stack was enclosed in an airtight box through which could be circulated dry argon to maintain a relative humidity of 60%. It was possible to enclose the magnet in a thermally insulated wooden structure and refrigerated water was circulated through cooling coils placed within. In this way a temperature was maintained of between 8 and 11°C. Only a small amount of additional shielding, in the form of lead sheet 1 cm thick placed around the sides of the pole gap, was necessary since the material of the magnet itself shielded the stack from above.

4.3 The Development of the Plates

In view of the apparently variable nature of the emulsion, a considerable effort was made to obtain a good and reproducible development.

With a temperature cycle method of development, the greatest problem

when sandwich plates are employed arises at the hot stage, where a rapid rise in temperature of some 20°C is required. Normally, glass-backed emulsions rest on a highly conducting metal surface, but for sandwich plates, conduction from the surrounding air is the sole means of heat transfer. Longer durations at the hot stage are therefore necessary but these lead to oxidation of the developer at the surface of the emulsion and eventually to total loss of the latent image. This latter effect had been experienced during the first experiments. The problem was solved by a wet hot stage of short duration before the normal dry one. For convenience, the plates were removed from the frames during the period of pre-soaking in cold water when the adhesive holding them had softened sufficiently. They were then placed in a perspex holder similar in design to a normal photographic plate holder; this made for much greater ease of handling. After a period of half an hour in a bath of developer at 4°C, the plates were placed for ten minutes in developer at 26°C; a dry hot stage at 24°C and of one hour's duration then followed. The remainder of the processing cycle was normal for emulsions of this type. Fixing in a 30% solution of 'hypo' occupied about two hours and then a slow dilution was begun at a rate of 3% per hour with constant agitation. After a thorough washing, the plates were plasticized in a 2% solution of glycerine for a short period and finally dried in a stream of air.

The improved development obtained with this technique served to emphasize a heavy fog present at the emulsion-glass interface. Various sources of contamination were looked for and many varieties of solution were tried for attaching the stripped emulsions to the glass, but with little success. It was found that the only certain way to eliminate the fog was to coat the plates directly with emulsion in the liquid phase. To avoid the recording of no-field particles in the two emulsions of a plate, a compromise was effected whereby the upper face (on which was inscribed the reference grid) was coated at Ilford and a stripped emulsion was affixed to the lower face immediately on return to Durham and shortly before the commencement of the exposure. This ensured that the fog would not interfere with the making of measurements from which the momentum would later be calculated.

4.4 The Examination of the Stack

Only the first and third exposures were examined in detail. A brief examination of the second revealed a very low density of tracks. Apart from the tedium and likely inefficiency of scanning in such a stack, in view of the length of the exposure the possibility of some fading having occurred could not be ruled out. Greater care was taken with the longest exposure of all, the fourth, and although a useful track density was obtained, distortion was of such a high order that it was almost impossible to recognize pairs of tracks: this exposure,

therefore, had also to be abandoned. Apart from slight oxidation of the surface of the emulsions, the first exposure was in every way successful, and it is from this that the bulk of the results have been obtained. With the third exposure, a slightly higher density of tracks was achieved but the improved development was marred by a more conspicuous fog at the interface due to the finer grain of the K5 emulsion. Despite the resulting poor conditions for microscopic observation, a small area was scanned in order to augment the statistics at zenith angles above 80°.

The method of examination has already been described (section 3.41). The efficiency of scanning for tracks in the first plate falls off rapidly with decreasing steepness of the track. This is both because the apparent ionization decreases and also because of the increasing distance away of the partner in the lower emulsion. A limit was set, therefore, to the displacement of the partner of ± 250 μm in the direction of magnetic deflection and ± 150 μm in the perpendicular direction with corresponding values of 28 and 17 μm for the length of the track in each emulsion. This limited the effective angular range of the spectrograph to $\pm 10^{\circ}$ in the zenithal direction and $\pm 15.8^{\circ}$ of azimuth.

A lower limit to the momentum was set of 800 MeV/c and this, together with errors of measurement and errors due to scattering in the first plate, determined the area of search in the second. For the

first gap of 1 cm in width this was a rectangle 700 x 300 μm^2. It was found necessary to scan a similar area of the third plate following the second gap of 2.54 cm, but after this the position of a track in the next plate could be predicted to within much less than a field of view.

The work of scanning was checked at every stage and it was found that all stages following the first recognition of a pair of tracks in one plate were carried out with very high efficiency. The efficiency of the first stage was determined by the rescanning of a given area a number of times by either the same or another observer. An alternative procedure was to scan a corresponding area in another emulsion and this took into account possible non-uniformities in the development. In this way the scanning efficiency was estimated with an error of about 14%.

Initial examination was made of five areas as shown in table 2.

TABLE 2

No. of scan	Exposure	Area in cm^2	No. of particles	Efficiency in %	
				Single	Repeated
I	1	4.62	246	67	91
II	1	3.99	281	72	91
III	1	3.81	187	76	93
IV	1	4.17	217	70	95
V	3	3.14	233	81	96

The separating boundaries of each area were lines of the reference grid, so that the co-ordinates of all particles found in one scan were referred to the same reference cross. The four areas of the first exposure were adjacent to each other and covered entirely the effective working area in the first plate. In the third exposure, because of the heavy fog already alluded to, the examination was carried out in the fourth plate where the best conditions of observation pertained. Where the area of scanning approached the edge of the plate, limiting criteria were introduced so that the trajectories of particles selected for tracing would not soon leave the stack. Allowance was made for the effects of these in the calculations. The total area of emulsion scanned is shown in the third column and in column four the total number of particles observed. About 6% of these were subsequently found to have momenta less than 1 GeV/c. The efficiencies for the regions of single and repeated scanning are given in the last two columns. About a third of the total area was scanned more than once. The figures are fairly constant over the five scans, those for the fifth scan being the highest. Here, despite the poor observing conditions, there was a higher density of tracks (as is apparent from the table) and slightly higher magnification was used.

4.5 The Determination of the Momentum

In order to calculate the momentum of a particle by the methods

outlined in section 2.2, it is necessary to relate the measured co-ordinates of the trajectory in any given plate to those in, say, the first plate as origin. This is done by means of the known relationships between the grids obtained from the calibration with the monocular microscope. However, in an experiment such as the present one, in which substantial numbers of particles are found with momentum greater than about a fifth of the MDM, these may be used to improve the accuracy of the optical calibration. The co-ordinates of the particle trajectories were measured relative to the nearest reference cross according to the area in which they were found. The co-ordinates of any trajectory whose lateral displacement in traversing the stack was greater than the distance between two crosses (2 cm) were adjusted so that they referred to corresponding crosses in each plate for the whole of the trajectory. A number of high energy particles were selected by inspection of the measured co-ordinates. The latter were referred to an axis obtained from the optical calibration and their first and second differences computed. Corrections to the calibration figures were calculated which would make the second differences minimal and the corrected values were fed back into a computer programme. The process was repeated as often as necessary and for each of the five scans. The method ensured that account would be taken of any small systematic errors between the calibration and subsequent measurements.

Having obtained accurate reference axes, the momenta of all particles were estimated on the digital computer by the least squares method of section 2.2. For those particles with momenta greater than about half the MDM, an estimate was also made of the error δs. For 108 selected particles with momenta greater than 20 GeV/c, the differences in each plate between the experimentally measured co-ordinates and the points fitted by the least squares method were obtained and their mean values found for each scan separately. None of the mean values was significantly different from zero, confirming that adequate reference axes had been found.

CHAPTER 5

THEORETICAL CONSIDERATIONS

5.1 Introduction

In order to obtain a theoretical estimate of the sea-level μ-meson intensity at large zenith angles, it is necessary to make some assumptions concerning its origin near the top of the atmosphere and propagation through it. Little is known directly of the nature, number and energy distribution of the secondary products of the interactions of the primary radiation; an estimation of the sea-level μ-meson spectra derived from the intensity of primary particles can therefore be in serious error owing to the number of assumptions which it is necessary to make. A more reliable estimate is obtained by employing the experimentally established spectrum of μ-mesons incident at sea-level from the vertical direction to determine the production spectrum of the parent mesons near the top of the atmosphere. Then from this spectrum with the same model of production and dissipation of the parent component is obtained the sea-level μ-meson intensity at large zenith angles. In this way it is possible to compare sea-level spectra at different zenith angles using a minimum number of assumptions concerning the origin of the mesons.

The derivation of the sea-level μ-meson intensity from an assumed production spectrum of π-mesons is fairly straightforward and has been treated by several authors (see, for example, Barrett et al, 1952; Murayama et al, 1956). However, a proportion of the μ-meson flux will originate from K-meson parents and to estimate this requires a more complex analysis since K-mesons have many different modes of decay. At K-meson energies of up to a few GeV, it is established that a majority of them decay into a single μ-meson accompanied by a neutral particle and this case may be treated in a similar way to that of the π-meson. Thus only one form of analysis is needed.

5.2 The Contribution of the π-meson Component

The derivation presented of the sea-level μ-meson spectrum follows that given by Barrett et al (1952).

It is assumed that the π-mesons are produced exponentially with production length λ_p, are dissipated through interaction with attenuation length λ_π and decay with mean lifetime τ_π. The unidirectional diffusion equation is then

$$\frac{d\pi(E^*,x,\theta)}{dx} = \frac{F(E^*)}{\lambda_p} \exp\left(-\frac{x}{\lambda_p}\right) - \pi(E^*,x,\theta,) \left[\frac{1}{\lambda_\pi} + \frac{B}{E^*\rho}\right] \qquad (9)$$

where $\pi(E^*,x,\theta)$ is the differential intensity of π-mesons of energy E^*

at a depth x (g cm^{-2}) and zenith angle θ, $F(E^*)$ the π-meson production spectrum, $B = m_\pi c/\tau_\pi$, and ρ is the atmospheric density at x.

A solution to this equation is given by

$$\pi(E^*,x,\theta) = F(E^*)\ \exp\left(-\frac{x}{\lambda_\pi}\right)\frac{x}{\lambda_p}\left\{\frac{1}{1+\frac{B}{E^*\rho}\frac{x}{}} - \frac{x\left(\frac{1}{\lambda_p}-\frac{1}{\lambda_\pi}\right)}{2+\frac{B}{E^*\rho}\frac{x}{}} + \frac{1}{2!}\cdot\frac{\left[x\left(\frac{1}{\lambda_p}-\frac{1}{\lambda_\pi}\right)\right]^2}{3+\frac{B}{E^*\rho}\frac{x}{}} - \ldots\right\} \qquad (10)$$

involving a series expansion in terms of $(1/\lambda_p - 1/\lambda_\pi)$. λ_p is determined experimentally and values are in the region of 120 g cm^{-2} (see, for example, Ticho 1952). The geometrical absorption length for π-mesons is about 60 g cm^{-2}, thus λ_π, the attenuation length, should have a value rather larger than this. Trefall (1957) has argued theoretically for $\frac{1}{2}\lambda_p < \lambda_\pi < 2\lambda_p$. As an approximation it will assumed that $\lambda_\pi \doteq 120$ g cm^{-2} since for the case $\lambda_\pi = \lambda_p$ all terms in the series expansion except for the first are equal to zero. Putting $\lambda_\pi = \lambda_p = \lambda$, equation 10 becomes

$$\pi(E^*,x,\theta) = F(E^*)\ \exp\left(-\frac{x}{\lambda}\right)\frac{x}{\lambda}\left[1+\frac{B}{E^*\rho}\frac{x}{}\right]^{-1} \qquad (11)$$

Provided that λ_π is not very different from λ_p, this is in any case a good approximation.

In deriving the μ-meson production spectrum from this equation, account must be taken of the fact that π-mesons of energy E^* give rise

to μ-mesons having a range of energies $E = E^*/r$ where $1 < r < (m_\pi/m_\mu)^2$. Calculations showed that the assumption of a unique energy of conversion given by $r = m_\pi/m_\mu = 1.32$ led to errors of the order of only 1%.

A summation of the π-mesons which decay within a depth x yields the μ-meson spectrum

$$M(E,\theta)\, dE = \int_0^x \frac{B}{E^* x} \frac{x}{\rho}\, \pi(E^*,x,\theta)\, dE^*\, dx \qquad (12)$$

The majority of the μ-mesons are produced within the first 500 g cm^{-2} where the variation of x/ρ is small. By assuming a constant value of x/ρ at each zenith angle equation 12 can be easily evaluated. Moreover, for sea-level spectra $x \gg \lambda$, consequently the upper limit of integration can be replaced by ∞. With these simplifications, the substitution of 11 in 12 gives

$$M(E,\theta) = r\, F(rE) \left[1 + \frac{rE}{B} \frac{\rho}{x}\right]^{-1} \qquad (13)$$

Using this spectrum and the survival probability the μ-meson spectrum at sea-level can be found. Both the survival probability and the energy at sea-level, however, are functions of the depth of production.

Since the production length of the π-mesons is about 120 g cm^{-2}, few μ-mesons will be produced below 300 g cm^{-2}. In the calculations

the proportion of μ-mesons produced at ten levels between 0 and 300 g cm^{-2} was estimated, assuming that their rate of production has an exponential dependence on the depth, and, with the value of ρ/x appropriate to each level, their contribution to the sea-level spectrum was found. It was subsequently found that the assumption of a single level of production of 120 g cm^{-2} led to an error of about 4%.

5.3 The Relationship between Density and Depth in the Atmosphere

The quantity of matter traversed by the particles was estimated by assuming a standard atmosphere in which the density ρ in g cm^{-3} is given by

$$\rho = h_o k \exp(-kz) \tag{14}$$

where h_o and k are functions of the vertical distance z. The distance y in an inclined direction is related to z by the approximate relation

$$z = y \cos\theta + y^2/2R \tag{15}$$

where R is the radius of the earth. The total amount of matter traversed is

$$x = \int \rho \, dy \tag{16}$$

Combining equations 14, 15 and 16 yields

$$x = \int h_o k \exp\left[-k(y \cos\theta + y^2/2R)\right] dy \tag{17}$$

The values of h_o and k were taken from Rossi (1952), p.544 and the relationship between x and y was computed for zenith angles between 60^o and 90^o at 2.5^o intervals. This was done by performing a numerical integration of equation 17 on a digital computer. For the purpose of subsequent calculations, values were obtained of y, x, and x/ρ at equal intervals of x to the extent of about 100 values at each zenith angle. Values of these quantities were also obtained for the ten assumed levels of production. The variation of x/ρ with x is shown in figure 6, the end point of each curve indicating the total atmospheric depth at that zenith angle. It will be seen that at zenith angles approaching 90^o the total depth increases very sharply and this affects radically the form of the μ-meson spectra at sea-level.

5.4 Energy Loss and Survival Probability

In traversing the large depth of atmosphere, the μ-meson sustains a considerable energy loss which is dependent on its energy. The assumed form for this loss is important because of the close dependence on it of the sea-level intensities. The sources of the energy loss are ionization, pair production, bremsstrahlung and nuclear interaction. Barrett et al have estimated the magnitude of these losses and their results have been modified by Jakeman for losses in air. The equation as given by Jakeman is

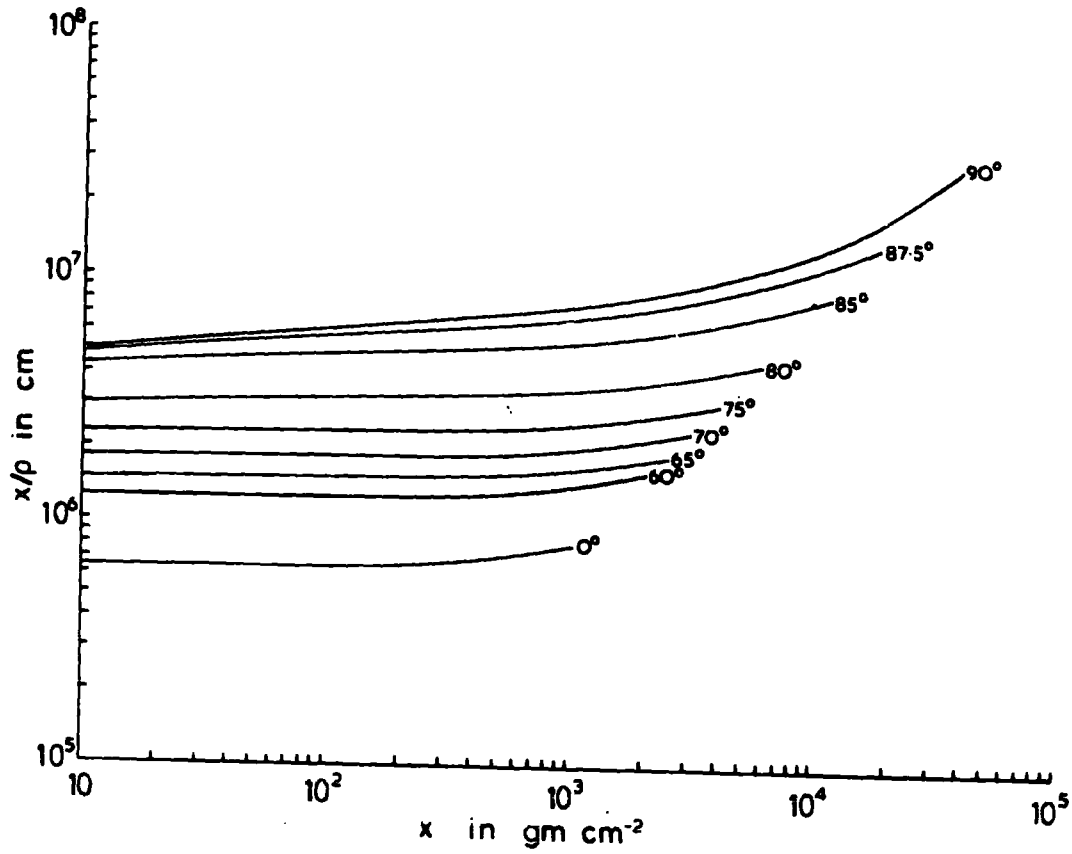

Fig.6. The variation of the quantity x/ρ with atmospheric depth x.

$$-\frac{dE}{dx} = 1.9\ 10^6 + 0.4\ 10^6 \log(E/m_\mu c^2) + 5.38\ 10^{-7}E \log 10^{-8}E \quad eV/g\ cm^{-2} \qquad (18)$$

More recently, however, for losses due to ionization, Sternheimer (1959) has deduced the equation

$$-\frac{1}{\rho}\frac{dE}{dx} = \frac{A}{\beta^2}\left[B + 0.69 + 2 \ln \frac{p}{\mu c} + \ln W_{max} - 2\beta^2 - \delta - U\right] \quad MeV/g\ cm^{-2} \qquad (19)$$

where for air, A and B have the values 0.0768 and 17.89 respectively, μ and p are the mass and momentum of the incident particle and W_{max} is the maximum energy transfer to an atomic electron. δ is the correction for the density effect, and U is the shell correction, unimportant at high energies. If the contributions of the remainder are estimated by making appropriate modification to the figures, which refer to rock, given by Ashton (1961), then the sum of these is

$$-\frac{dE}{dx} = \left[1.04 \ln(E/\mu c^2) + 15.5\right] 10^{-7}E \quad MeV/g\ cm^{-2} \qquad (20)$$

Ashton has correlated the range-energy relation for μ-mesons deduced from these equations with measurements of the underground depth-intensity curve and found no significant disagreement.

The total losses calculated by means of equations 19 and 20 agree with values obtained from equation 18 for energies above about 20 GeV; at 1 GeV the discrepancy is about 12%. Thus an adaptation of Jakeman's equation

$$-\frac{dE}{dx} = 1.09 + 0.174 \ln E + 2.335\ 10^{-7} E \ln 10^{-2} E \qquad \text{MeV/g cm}^{-2} \qquad (21)$$

was used for energies above 200 GeV where the variation is most complex and, below, the simpler empirical formula

$$-\frac{dE}{dx} = 0.14 + 0.274 \ln E \qquad \text{MeV/g cm}^{-2} \qquad (22)$$

which reproduces the form of the calculated variation.

A certain fraction of the μ-mesons produced at the top of the atmosphere decay before reaching sea-level. The survival probability $w(y_1 y_2)$ for a μ-meson produced at a depth y_1 to reach the depth y_2 is given by

$$-\ln w(y_1 y_2) = \int_{y_1}^{y_2} m_\mu c/\tau_\mu E \, dy \qquad (23)$$

Both the energy loss and survival probability are functions of the energy E. The two quantities were computed simultaneously therefore from the known relationships between x and y at each of the 100 intervals of the atmosphere. For particles of a given energy at production, estimation was made of the quantity

$$\sum_{i=1}^{n} \left[E_i - \left(\frac{dE_i}{dx_i}\right) \Delta x_i \right]$$

which is the energy at sea-level, and of

$$m_\mu c/\tau_\mu \sum_{i=1}^{n} \Delta y_i / \left[E_i - \tfrac{1}{2}\left(\frac{dE_i}{dx_i}\right) \Delta x_i \right]$$

which is the survival probability at sea-level. To achieve the best estimate of the latter quantity, the mean energy $E_i - \frac{1}{2}\left(\frac{dE_i}{dx_i}\right) \Delta x_i$ in each interval was used. Δx_i and Δy_i are the differences between successive values of the 100 estimated as described in the previous section. It was found that the most convenient way of performing the computations was to assume a suitable value for the sea-level energy and calculate the energy at production for each of the ten levels with positive signs replacing the negative ones in the above expressions.

Typical variations of the total energy loss with zenith angle are shown in figure 7 for μ-mesons produced at 120 g cm^{-2} and with various energies at sea-level. The corresponding variation of the survival probability is shown in figure 8. The shape of the curves for low energy mesons at zenith angles above 85° can be understood by reference to figures 6 and 7. The rapidly increasing depth of atmosphere at these angles results in a greatly increased energy loss and consequently a higher energy at production. It will be seen, for example, that the production energy is twice as great at 90° as it is at 87.5° for sea-level energies of up to 16 GeV. Because of the greater mean energy over the path through the atmosphere, the survival probability at 90°

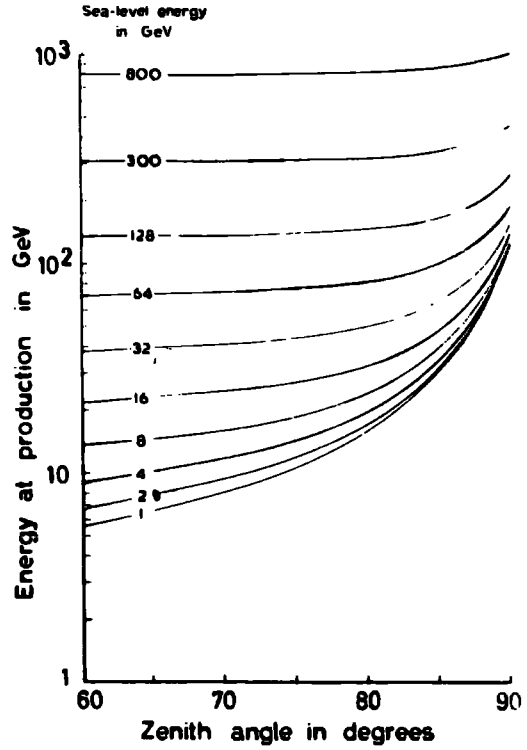

Fig. 7. The variation with zenith angle of the energy of μ-mesons at production.

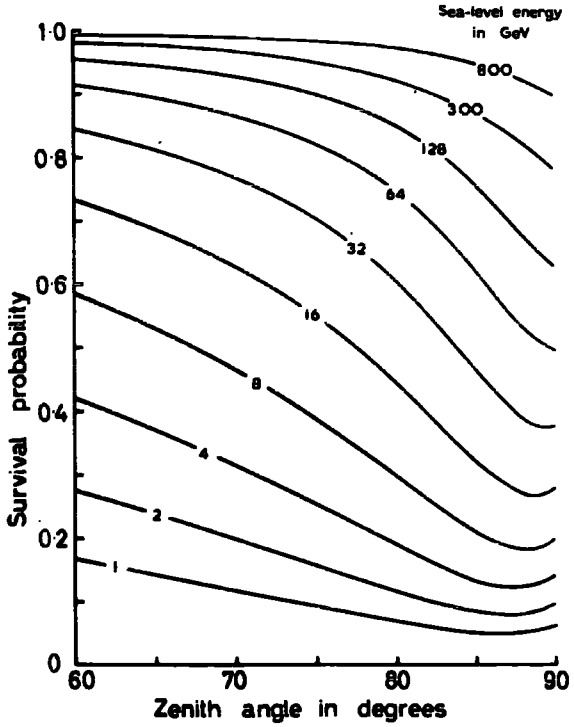

Fig. 8. The variation with zenith angle of the survival probability of μ-mesons.

is slightly higher than at 87.5° despite the increase in atmospheric depth.

5.5 Corrections to the Sea-level Spectra

The unidirectional approximation assumes that the primary particles arrive isotropically at the top of the atmosphere and that the π-mesons and μ-mesons do not deviate from their direction of production.

At large zenith angles μ-mesons having energies of a few GeV at sea-level come from π-mesons of considerably greater energies. If the distribution of primary particles is isotropic, then the secondary π-mesons will also have an isotropic distribution and their angular spread during production can be ignored. It can be shown that the maximum angle of the π-μ decay is given by

$$\sin \theta_{max} = \tfrac{1}{2}\left(\frac{m_\pi}{m_\mu} - \frac{m_\mu}{m_\pi}\right) \frac{m_\pi c}{p_\pi} \qquad (24)$$

where p_π is the momentum of the π-meson. For the extreme case of a μ-meson of energy 1 GeV at sea-level incident from the vertical direction, this yields a value for θ_{max} of about $\frac{1}{2}°$. Thus angular spread of the μ-mesons may also be ignored.

Correction must be made for the effect of different cell widths, which arises where the energy loss through the atmosphere is comparable

in magnitude with the energy of the meson. In this case the width of an energy interval considered at sea-level corresponds to a greater interval at the level of production. Corresponding values of the two energies were plotted and the correction found from the slope of the curve. Above 20 GeV it was negligible and the maximum value, at the lowest energy considered (3 GeV), was 0.88.

There are, however, two further corrections that are relatively important.

5.51 Geomagnetic Deflection

For μ-mesons with an energy of only a few GeV, deflection in the earth's magnetic field results in an increased path length through the atmosphere with a consequent increase in energy loss and reduction in their survival probability at sea-level.

The geomagnetic deflection may be calculated very simply. Values of 0.168 and 0.475 gauss were assumed for the horizontal and vertical components of the earth's magnetic field over the average path through the atmosphere. The values were taken from Curves of Equal Magnetic Variation, 1960, published by the Admiralty. The deflection of the trajectory due to the component of the field perpendicular to it was calculated in each of the 100 intervals and the total deflection, energy loss and survival probability estimated. The variation of the total angle of deflection with the sea-level energy of the meson is

shown in figure 9 for four different zenith angles: the shape of the curve at 90° is again a consequence of the greatly increased energy loss. However, although the deflection is quite large at low energies, the resulting increase in path length is not very great and the effect on the sea-level intensities at energies of more than 5 GeV is less than 1%. At 1 GeV there is a decrease in intensity of 2% at 65° zenith angle, 3% at 75° and 5% at 85°.

5.52 Scattering

Scattering of the μ-meson can be considerable and this produces a relative enhancement of the low energy intensity at large zenith angles. Since the intensity decreases rapidly with increasing zenith angle, the number of scattered mesons received in any given angular interval from smaller zenith angles is greater than that lost to it. An approximate correction was made for this effect. A more exact method would be to correct the intensities at intervals through the atmosphere using the appropriate values of the r.m.s. angle of scattering. As this involves laborious computation, a mean overall correction was made.

The variation with zenith angle of the intensity I of particles with one particular energy was approximated to an expression of the form $I = I_0 \exp -k(\theta)$. If the r.m.s. angle of scattering is σ then it can be shown (Lloyd and Wolfendale, 1955) that, for values of $\theta \gg \sigma$,

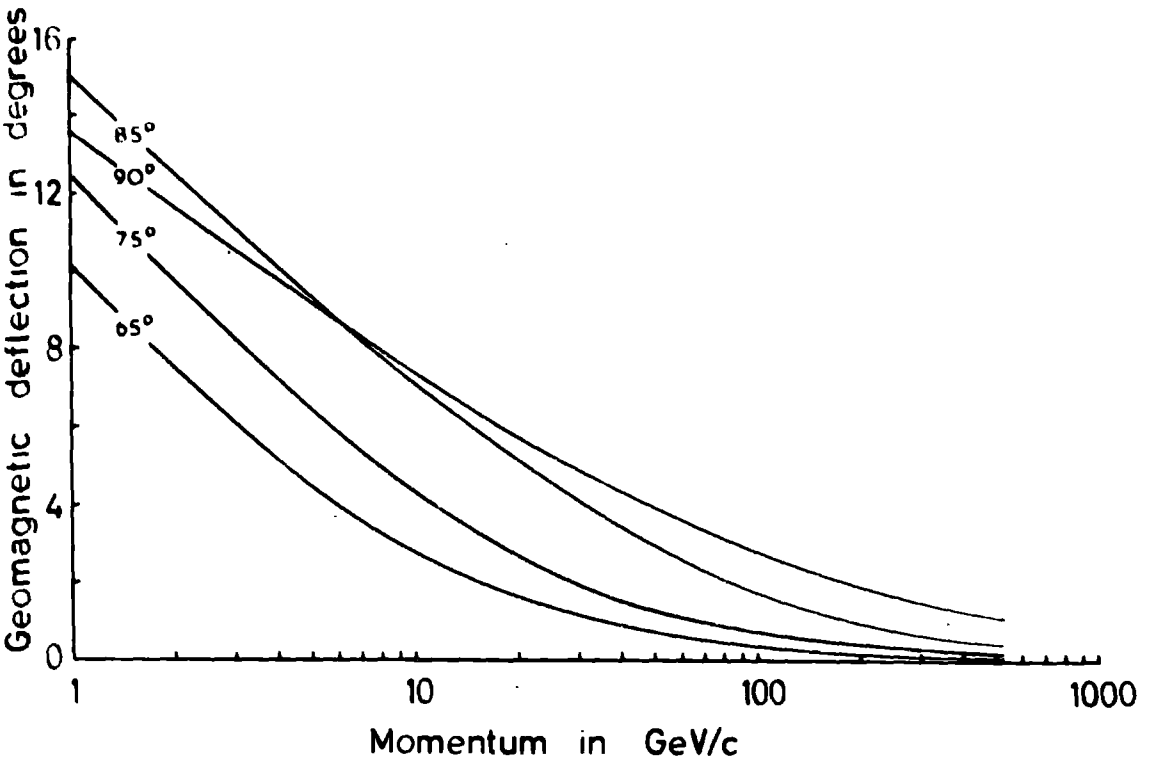

Fig. 9. The variation of geomagnetic deflection of μ-mesons with momentum.

the intensity I_s corrected for scattering is given by $I_s = I \exp(k^2 \sigma^2/2)$. The mean square projected angle of scattering $\overline{\sigma^2}$ in a small thickness Δx and at high energies is given by (Rossi, p.68)

$$\overline{\sigma^2} = \frac{E_s^2}{X_o} \frac{\Delta x}{E^2} \qquad (25)$$

where $E_s = 21$ MeV and $X_o = 37.7$ g cm^{-2} (the radiation length in air). The r.m.s. angle of scattering was computed for a series of energies up to 32 GeV by summing contributions estimated from equation 25. Small intervals, Δx , were considered and the mean energy E_i in each interval, allowing for energy loss, was used. Since the angle of scattering is inversely proportional to the energy, most of the scattering will take place near sea-level where the rate of loss of energy is also large. The intervals Δx , therefore, were made increasingly small towards sea-level. The results are plotted in figure 10. Since σ is a function of x, the r.m.s. angle of scattering varies with the height of production of the μ-mesons; it has already been assumed, however, that these are all produced within the first 300 g cm^{-2} and over this region the variation in σ is negligible. It may also be noted that σ is inversely proportional to the magnitude of the energy loss. Thus, for example, for a 1 GeV particle at sea-level and 85° zenith angle, the formula given by Jakeman yields a value of 2.76° for σ compared with 3.94° from figure 10. The corresponding corrected intensities

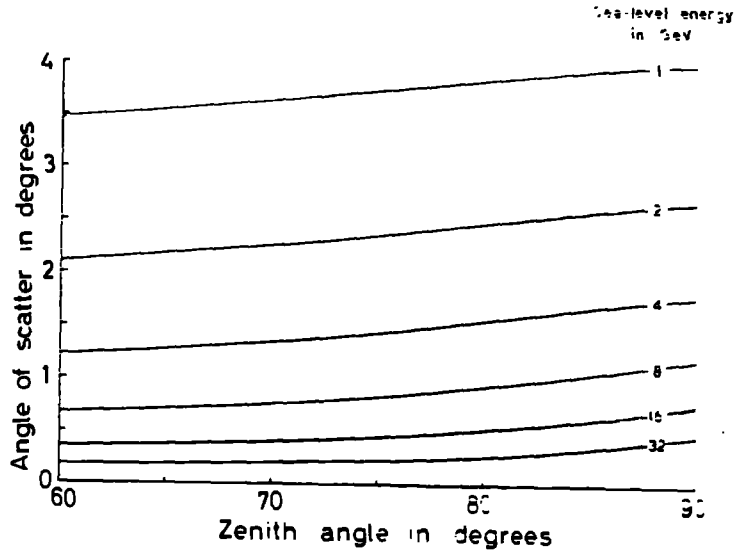

Fig.10. The r.m.s. angle of scattering plotted as a function of zenith angle

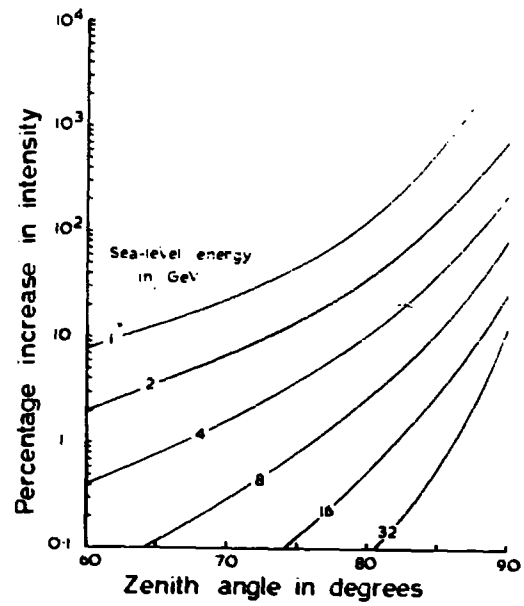

Fig.11. The effect of scattering on the sea-level intensities.

are 1.8 10^{-6} and 4.5 10^{-6} (particles/cm^2 sec GeV/c).

The effect of scattering on the sea-level intensities is shown in figure 11. It will be seen that it increases markedly above 80° on account of the rapid variation of intensity with zenith angle and this variation is in consequence considerably lessened. The only other estimation of the scattering correction has been carried out by Maeda (1960), who has calculated the r.m.s. angle of scattering at 30° and 60° to the zenith. He obtains at 60° for μ-mesons with an energy of 1 GeV at sea-level a value of about 3.7°, which compares well with that shown in figure 10. However, by expressing the sea-level μ-meson intensity as a function of zenith angle with the r.m.s. angle of scattering as a small correction and with numerical evaluation of the differential coefficients of the resulting Taylor series expansion, he estimates that this will result in an increase in the sea-level intensity of about 250%, a value very much higher than is obtained from figure 11.

5.6 Sea-level Spectra at Large Zenith Angles

By means of the foregoing analysis a π-meson production spectrum $F(E^*)$ was fitted to the vertical spectrum of Ashton et al (1960). For π-meson energies between 10 and 1000 GeV, $F(E^*)$ was of the form $I_0 E^{*-\gamma}$ where $I_0 = 0.425 - 0.125 \log_{10} E^*$ and $\gamma = 3.92 - 0.944(1 - 0.125 \log_{10} E^*)^{-1}$ both being functions of the energy E*(GeV). The total uncertainties on

I_o and γ are about 10% between 10 and 100 GeV; at higher energies the error is greater because the determination of the vertical sea-level spectrum is much less certain. An approximate expression with constant I_o and γ is $I = 0.15\ E^{*-2.55}$.

With this spectrum and the appropriate values of (x/ρ), energy loss, survival probability and the various corrections, the sea-level spectra were computed for a range of zenith angles and some are shown in figure 12. They are valid only for particles approaching along the North geomagnetic meridian. To illustrate the magnitude of the scattering correction the uncorrected spectra at certain angles are indicated by broken lines.

The spectra given refer to zero azimuthal angle ϕ, and are corrected for geomagnetic deflection. At any other angle ϕ the intensity $I(\phi,\theta_1)$ can be shown to be approximately equal to the intensity for $\phi = 0$ at a larger zenith angle θ_2 where $\cos\theta_2 = \cos\theta_1 \cos\phi$. This approximation is valid when geomagnetic deflection is negligible, otherwise the intensity must be estimated numerically for all values of ϕ. For sea-level energies less than 16 GeV the variation of intensity with ϕ was computed and an extreme form of the variation is shown in figure 13 for 1 GeV μ-mesons at 85^o.

It will be observed that the intensities are symmetrical about $\phi = 0$ for positive and negative particles and that the maximum intensity, corresponding to the shortest atmospheric path, is at some value of

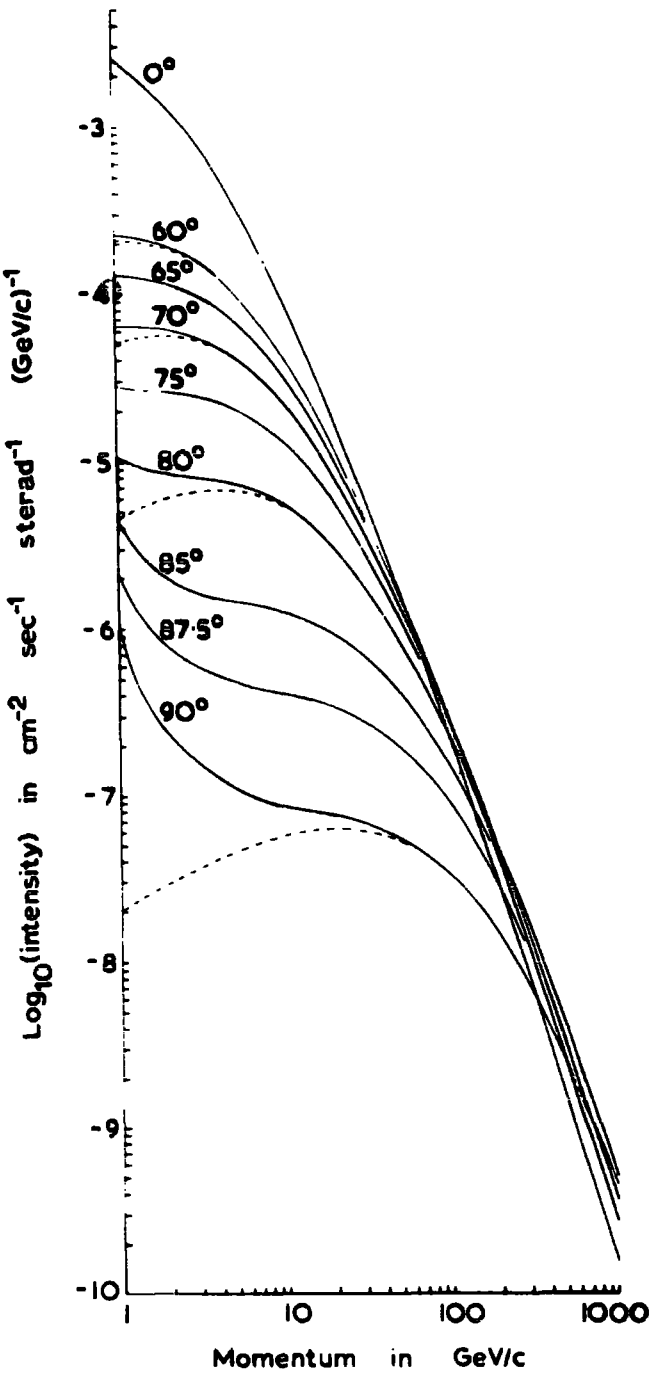

Fig.12. The differential momentum spectrum of μ-mesons incident at sea-level from geomagnetic North. The broken lines show the spectrum uncorrected for scattering.

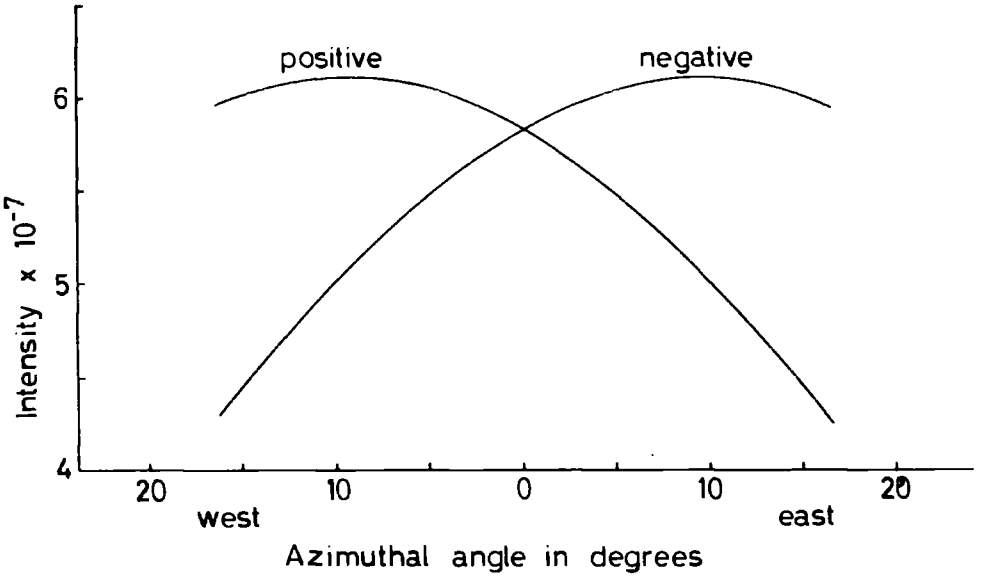

Fig.13. The variation of the sea-level intensity of 1 GeV/c μ-mesons with azimuthal angle at a zenith angle of 85°.

$\phi > 0$. For higher energies or smaller zenith angles, the maximum occurs at smaller values of ϕ. When the effects of geomagnetic deflection are ignored, the curves for positive and negative particles coincide, with the maximum intensity at $\phi = 0$, and are symmetrical about that point.

5.7 The Contribution of the K-mesons

It is not possible to take into account exactly the entire K-meson contribution since those that decay to a π-meson, for instance, will be already included in the π-meson production spectrum. It is of interest, nevertheless, to see what is the effect of direct production of μ-mesons by K-mesons, and in fact the $K_{\mu 2}$-meson is expected to be the most frequent type.

It has already been pointed out that a similar analysis may be applied to the case in which the $K_{\mu 2}$-meson is assumed to be the sole progenitor of the μ-meson component. However, in view of the large range of energies which a K-meson may have in giving rise to a μ-meson of energy E, namely from E to 22E, the simplifying assumption of a unique energy of conversion cannot be employed. Instead, it was assumed that the angular distribution of the decay particles was isotropic in the centre of mass system. The region between 0° and 180° was divided into six equal intervals and the mean energy of μ-mesons emitted in

each interval was calculated. The inverse distribution was taken to represent the energy range of K-mesons giving rise to μ-mesons of a single energy and a summation was made of the contributions from each interval. It was assumed, in the absence of any direct information, that $\lambda_p = \lambda_K$. Since the coupling constants for the interactions involving the production and absorption of K-mesons are the same, it is unlikely that λ_p and λ_K are very different from each other and even so the analysis will be a fair approximation. The mean height of production may be slightly different but this would not affect the result very much. A single level of production at 120 g cm^{-2} was assumed and this simplification introduced an estimated error of 4%.

A simplified production spectrum taking the form $F(E^*) = 0.2\ E^{*-2.55}$ was fitted to the vertical spectrum and with it the sea-level intensities at large zenith angles were estimated. The intensities so obtained closely resemble those for π-meson parents shown in figure 12; the greatest difference is at low energies where the curves derived from the K-meson analysis are some 10 - 15% higher. In the analysis $K_{\mu 2}$-mesons were regarded as being the sole parents: if a realistic proportion of K-mesons is taken and all modes of decay considered, the difference in intensities becomes very small.

Jakeman also estimated the effects of K-mesons although at the time only very approximate values were available of their masses and

lifetimes. He found that their presence would reduce the sea-level intensity at 90° to the zenith and by a factor of up to about two. It seems probable, however, that he employed the same form of production spectrum for both π- and K-meson parents and this would lead to an inaccurate result. He further assumed that a K-meson would on average give rise to a μ-meson having one third the energy of its parent and as explained above this must also give rise to some error.

It may be noted that although the effect of the K-meson component on the sea-level μ-meson intensities is small, at production it takes a significant proportion of the energy of the primary particles. An accurate energy balance of the cosmic radiation, therefore, must take into account this component.

CHAPTER 6

THE RESULTS OF THE SECOND SERIES OF EXPERIMENTS

6.1 Introduction

A total of 1097 particles with momenta greater than 1 GeV/c were observed between zenith angles of 65.3° and 85.0°. The momenta of these particles were computed by a least squares method as described in section 2.2 and their angle of arrival was calculated to within 0.1°; this accuracy was necessary on account of the rapid variation of intensity with zenith angle. Because of the low statistics the results were grouped into suitable intervals of momentum and zenith angle.

For the purpose of comparison with theoretical predictions it is assumed that all the particles observed are μ-mesons. The intensity of π-mesons of comparable momentum at sea-level is expected to be negligible. The intensity of protons arriving from the vertical direction is about 5% of the μ-meson intensity at 1 GeV/c and it decreases rapidly with increasing momentum. At large zenith angles it is expected that the number of protons will be an even smaller fraction than in the vertical direction.

6.2 The Differential Momentum Spectra

To compare the observed rates with the expected ones the following procedure was adopted. First the expected intensities were integrated numerically over the appropriate limits of azimuthal angle and graphically over zenith angle in intervals of 2.5°. A subsequent integration was carried out over momentum, the limits being chosen so that the rates (particles/cm^2 sec) were of similar statistical weight at each interval of zenith angle. The experimental rate was calculated separately for each of the five scans, taking into account the particular efficiencies and limiting conditions, and a simple mean calculated, since similar numbers of particles were observed in each area scanned.

The expected values and the observed rates are shown in figure 14. The solid lines refer to mean values of the π-meson production spectrum, their length indicating the limits of integration over momentum, and they have an uncertainty of about 10%. The errors on the experimental points have been obtained by combining the statistical error with the error in efficiencies of scanning; the area and the time of exposure are known to within a fraction of 1%.

The shape of the observed distributions is affected by uncertainties in the determination of momentum and a suitable measure of these is obtained from the signal to noise ratio. If S_y is the observed sagitta in the y-direction (due entirely to scattering) and S_x is the observed

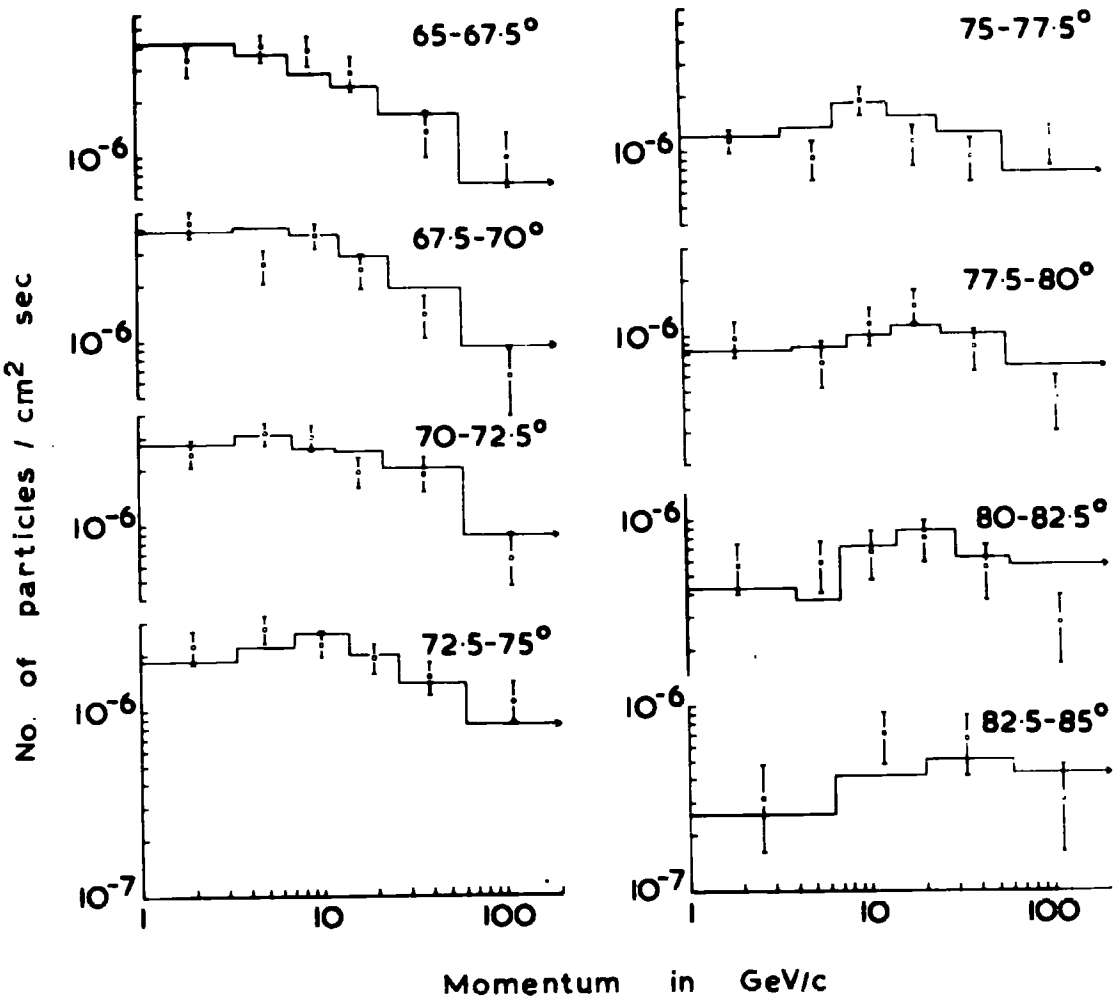

Fig.14. The differential rates of cosmic rays at sea-level.

magnetic sagitta (including scattering), then, in the region where scattering predominates and $\beta \doteq 1$, the ratio S_y/S_x is independent of momentum and it can be shown that

$$\text{variance } (S_y/S_x) = 1/R_o^2 \qquad (26)$$

where R_o is as defined in section 2.1. At the same time as the true momentum of each particle was computed, a calculation was made of the 'momentum' in the y-direction. For about 150 particles selected randomly in the region where equation 26 holds, the ratio of these two quantities was calculated and the variance of their distribution obtained. This gave a value of $(15 \pm 1)\%$ for $1/R_o$ which is in good agreement with one of 16% estimated from curves given in I. The curves refer to the three point method but a correction may be made for the increased accuracy of the method of least squares.

To determine the MDM, estimation was made from the calculated values of δs of the mean square value of δ for all particles of momentum greater than 40 GeV/c. Despite the limiting criteria employed when scanning near the edge of the emulsion in the first plate, not all of these particles passed through every plate of the stack. The value of the MDM decreases fairly rapidly as the number of points of observation is decreased. However, most of the 82 particles in this category were observed in all seven plates and all but 4 of the remainder in at least five. Making allowance for the effect of this, the r.m.s. value of δ

was found to be 5.45 ± 0.57 μm, which with equation 8 (section 2.2) implies a value of slightly more than 100 GeV/c for the MDM.

From these values of the noise to signal ratio, it was estimated that the spectra would be appreciably affected above 30 GeV/c. A correction was applied to the expected distributions by dividing the two large intervals 30 - 60 GeV/c and 60 - 300 GeV/c into smaller intervals of momentum and, from the known error on the momentum in these intervals, estimating their individual contributions to each of the two large intervals.

6.3 The Integral Spectrum

It is of interest also to compare the integral experimental rates with the theoretical curve. Since the statistics are rather poor, a better idea is obtained of the degree of agreement from such a comparison.

The integral rates above 1 GeV/c were estimated and are shown in figure 15. Since, in order to avoid any bias from the scanning and tracing of long tracks, the rates for the extreme intervals refer to a smaller azimuthal angle of $\pm 12.5^{\circ}$, the results have been plotted as the number of particles per steradian so that a smooth curve might be obtained. It will be seen that the agreement is very good: it must be emphasized that the curve and the experimental points are entirely independent and there is an error of about 10% on the theoretical curve.

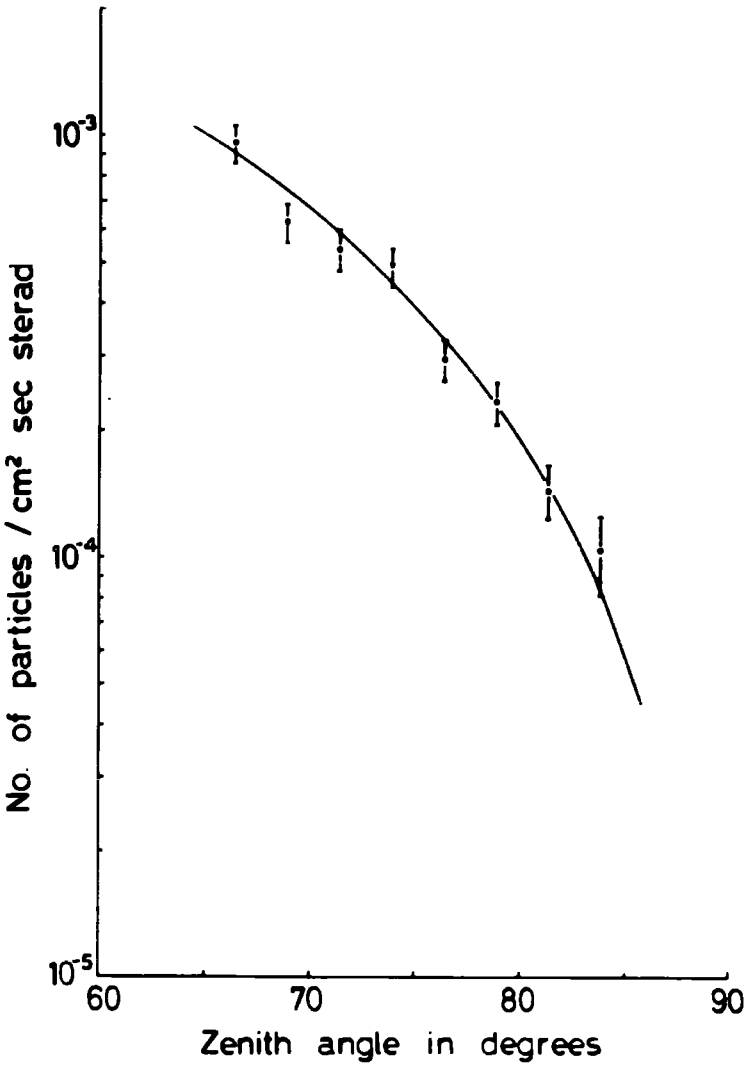

Fig.15. The variation with zenith angle of the integral rate of cosmic rays at sea-level.

In view of this it was thought unnecessary to apply any formal statistical test. It is difficult to allow for the two independent errors of theory and experiment, and, since no normalization is applied, a simple χ^2 test is not appropriate.

It was explained in section 4.4 that only 20% of the total number of particles were obtained from an exposure in which it was possible to observe particles arriving from zenith angles of greater than 85°. In the interval $85 - 87.5^\circ$, three particles were observed, all with momenta between 10 and 20 GeV/c, coinciding with the expected peak in the momentum distribution. The estimated rate is $(3.0 \pm 1.7)\ 10^{-5}$ particles/cm^2 sec sterad which is close to the expected value of $3.8\ 10^{-5}$. Between 87.5° and 90° no particles were observed where 1 - 2 might have been expected: again there is no significant disagreement.

6.4 The Positive to Negative Ratio

The variation of the positive to negative ratio with zenith angle and momentum is presented in table 3; the results have been grouped in intervals of 5° of zenith angle.

TABLE 3

Zenith Angle	65 - 70°	70 - 75°	75 - 80°	80 - 85°
Momentum in GeV/c				
1 - 7	1.96 ± 0.34	1.45 ± 0.23	1.52 ± 0.36	1.4 ± 0.6
7 - 22	1.78 ± 0.33	1.32 ± 0.22	1.08 ± 0.21	0.9 ± 0.3
> 22	1.36 ± 0.36	1.02 ± 0.22	1.54 ± 0.40	1.1 ± 0.4
> 1	1.78 ± 0.20	1.30 ± 0.13	1.30 ± 0.17	1.04 ± 0.22

The mean value over all angles and momenta is 1.39 ± 0.08.

It will be seen that the results for the interval 65 - 70° are above the value (~ 1.25) obtained by Pak et al (1961) to the extent of about 2.5 standard deviations. These authors found no significant difference between the ratio determined at 68° zenith angle and that in the vertical direction; they therefore combined their results for the two angles to improve the statistical accuracy. They do not state, however, at what angle of azimuth their results at 68° were measured and a direct comparison is perhaps not justified. Nevertheless, no explanation of this difference has been found in terms of experimental errors. In the first stage of scanning it is not possible to discriminate against particles of one particular sign and subsequent stages have

been thoroughly checked for the presence of bias of this type. The difference cannot arise from evaluation of the momentum, because an overestimation of the number of particles is possible only if a large error is present in the system of reference: this is ruled out by the method used in confirming the calibration figures. In addition, for an exposure in the North to South direction the magnetic field of the earth is not expected to interfere with the relative intensities of positive and negative particles. At about 70° zenith angle the deflection is confined entirely to the azimuthal plane and affects only the left to right asymmetry to a small extent. The existence of this asymmetry is confirmed by the experimental observations since the value of the left to right ratio for positive particles is 1.15 ± 0.09 and the equivalent right to left ratio for negative particles is 1.17 ± 0.11.

CHAPTER 7

DISCUSSION AND CONCLUSIONS

It has been shown how a compact device such as an emulsion spectrograph can be used successfully to measure cosmic ray spectra at sea-level over a useful range of momentum. With a greater magnetic field or a larger stack, and by remeasuring the trajectories of high energy particles with greater accuracy, it would be possible to increase the MDM to at least 500 GeV/c. The limit of 100 GeV/c was, however, quite adequate for the present investigation owing to the small number of particles, about 4% of the total, with momenta greater than 100 GeV/c. At zenith angles approaching 90°, of course, such particles constitute a greater and more important fraction of the total intensity.

The experimentally determined differential and absolute rates shown in figures 14 and 15 respectively agree well with the estimated values. The significance of the agreement is even greater when it is remembered that the present measurements are of absolute rates and do not require normalization. This demonstrates that the theoretical treatment outlined in Chapter 5 fully represents all processes involved within the experimental errors, which are of the order of 20%.

The experimental statistics obtained at zenith angles above 85°

were very poor. However, because of the low intensity of μ-mesons at these angles, the accumulation of a useful track density would require an exposure time of many months, a duration prohibited by considerations of fading in the emulsions. Such an investigation should be undertaken with counter techniques.

The rather high experimental value of the positive to negative ratio is a little disturbing, but at present an explanation in terms of statistical fluctuation is the only one that can be offered.

In order to employ measurements of spectra at large zenith angles as a means of discrimination between the π- and K-meson components, it is apparent from the discussion of section 5.7 that the total errors should not be greater than 3 - 4%. The attainment of such accuracy requires the accumulation of high experimental statistics and a far more exact theoretical analysis. The present technique, despite its advantage of permitting absolute measurements, is tedious in operation. Although the construction of a stack is not difficult and little attention is required during the exposure of it, examination is a very lengthy process, proceeding in the present case at a rate of about 100 particles traced through the stack per month. Although with practice and diligence this figure could no doubt be improved upon a little, it appears that further investigation of this particular problem must also be carried out in experiments employing counter

techniques. Present evidence (Keuffel et al., 1957; Kocharyan et al., 1960) suggests in any case that the proportion of K-mesons produced is at most some 15% of the π-meson intensity and probably very much less: to detect the effect of this proportion of K-mesons on the sea-level μ-meson spectrum will require a very precise technique.

ACKNOWLEDGEMENTS

The author wishes to thank Professor G.D.Rochester for his unfailing encouragement and advice. It is a pleasure for him to express his indebtedness to Dr. A.J.Apostolakis for his close co-operation throughout the period of the experiments. He wishes further to thank Dr. A.W.Wolfendale for useful discussions in the early stages of the experiment, and the staff of the University Computing Laboratory, Newcastle-upon-Tyne, for the provision of facilities. The D.S.I.R. are thanked for the provision of a research award and for grants without which the work could not have been carried out.

REFERENCES

Apostolakis, A.J. 1956 Ph.D. Thesis, University of Manchester

Apostolakis, A.J. and Macpherson, I. 1957(a) Proc. Phys. Soc. A, 70, 146

Apostolakis, A.J. and Macpherson, I. 1957(b) Proc. Phys. Soc. A, 70, 154

Ashton, F. 1961 Proc. Phys. Soc. 77, 587

Ashton, F., Brooke, G., Gardener, M., Hayman, P.J., Jones, D.G., Kisdnasamy, S., Lloyd, J.L., Taylor, F.E., West, R.H. and Wolfendale, A.W. 1960 Nature, 185, 364

Barrett, P.H., Bollinger, L.M., Cocconi, G., Eisenberg, Y. and Greisen, K. 1952 Rev. Mod. Phys. 24, 133

Caro, D.E., Parry, J.K. and Rathgeber, H.D. 1951 Aust. J. Sci. Res. A, 4, 16

Jakeman, D. 1956 Can. J. Phys. 34, 432

Keuffel, J.W., Morris, G.J., Stiff, R.K., Call, R.L. and Sandman, W.H. 1957 Phys. Rev. 108, 1584

Kocharyan, N.M., Kirakosyan, Z.A., Sharoyan, E.G. and Pikalov, A.P. 1960 Soviet Physics (J.E.T.P.) 11, 12

Lloyd, J.L. and Wolfendale, A.W. 1955 Proc. Phys. Soc. A, 68, 1045

Maeda, K. 1960 J. Atmos. Terres. Phys. 19, 184

Moroney, J.R. and Parry, J.K. 1954 Aust. J. Phys. 7, 423

Murayama, T., Murakami, K., Tanaka, R. and Ogawa, S. 1956 Prog. Theor. Phys. 15, 421

Owen, B.G. and Wilson, J.G. 1951 Proc. Phys. Soc. A, 64, 417

Pak, W., Ozaki, S., Roe, B.P. and Greisen, K. 1961 Phys. Rev. 121, 905

Pine, J., Davisson, R.J. and Greisen, K. 1959 Nuovo Cimento, 14, 1181

Rossi, B. 1952 High-Energy Particles, New York; Prentice-Hall, Inc.

Smith, J.A. and Duller, N.M. 1959 J. Geophys. Res. 64, 2297

Sternheimer, R.M. 1959 Phys. Rev. 115, 137

Ticho, H.K. 1952 Phys. Rev. 88, 236

Trefall, H. 1957 Physica, 23, 65

Wilson, B.G. 1959 Can. J. Phys. 37, 19